Melt inclusion chemistry and associated Cu-Mo-Au mineralization in 2.7-Ga porphyry intrusions and volcanics, Timmins, Ontario

By

Abdul Wahab Israr

A Thesis Submitted to

Saint Mary's University, Halifax, Nova Scotia

in Partial Fulfillment of the Requirements

for the Degree of Bachelor of Science, Honors in Geology

April 28th, 2017, Halifax, Nova Scotia

Approved: Dr. Jacob Hanley
Associate Professor

Melt inclusion chemistry and associated Cu-Mo-Au mineralization in 2.7 Ga porphyry intrusions and volcanics, Timmins, Ontario

By: Abdul Wahab Israr

April 28, 2017

Abstract

Melt inclusions are tiny samples of melt that are trapped by crystals growing in a magma. In this study, melt inclusions hosted in quartz phenocrysts from the Paymaster Porphyry, Crown Prophyry and Krist fragmental unit, Timmins, Ontario, were analyzed to provide a better understanding of the processes involved in compositional evolution of Archean porphyry magmas. Laser ablation inductively coupled plasma mass spectrometry (LA-ICP-MS) analyses of the melt inclusions as well as Back Scattered Electron – Scanning Electron Microscopy (BSE-SEM) analyses of mineral surfaces from the Pearl Lake porphyry were used to further investigate the behaviour of Cu, Mo and Au. The mineralogy of the porphyry rocks from four localities comprises mostly quartz (~25-35%), seriticized plagioclase (~20-40%), seriticized K-feldspar (~15-20%), chloritized biotite (<5%), calcite (~5%) and trace amounts of chalcopyrite.

SEM data shows that Cu and Au coprecipitated in the porphyry ores and this implies that Cu and Au are genetically related; therefore, any processes that influenced Cu enrichment might have also influenced Au. The melts from the Paymaster and Crown porphyry along with the Krist fragmental fall in the adakitic field (high Sr/Y, low Y and high $La/Yb_{(N)}$, low $Yb_{N)}$. The adakitic evolutionary trend that is shown by these melts cannot be portrayed by bulk rock analyses as they are limited in compositional range and implies fractionation of metals at depth. Paymaster and Crown porphyry melt inclusion compositions along with those from the Krist fragmental unit demonstrate that the melts in these intrusive systems were sourced from the same parental liquid, but show some differences in Cu-Mo-W-As-Sb-Ag-Bi and Sn.

The adakitic trend is further supported and illustrated by other geochemical discriminations, such as the Yb/Ta discrimination diagram which places the melts in the VAG field, confirming that the three localities are most consistent with orogenic volcanic arc granite setting. A TAS classification diagram places the bulk composition of the melts mainly in the dacite field. The melt inclusion data shows that the magmatic history of the system is protracted since the porphyry melts are compositionally similar over a ~10 Ma window of intrusion + fragmentation (Krist) and intrusion (Paymaster + Crown). $(Yb)_N$ vs $(La/Yb)_{N,}$ Y and Cu vs Sr/Y and Nb/Ta vs Zr/Hf plots illustrate a relationship showing the fractionation of elements and the evolution of metals, as the Nb, Ta and Cu concentrations seem to be following trends that are not necessarily explained by the crystallization of minerals in a chamber at depth, but instead possibly inform us about magma degassing in the Archean. This study confirms that melt inclusion analyses conducted on Archean age rocks can quantify metal contents

Table of Contents

1.0 Introduction.....5

1.1 Archean lode gold deposits.....5

1.2 Archean mesothermal gold deposits.....6

1.3 Regional geological setting of Timmins, Ontario.....9

1.4 Tisdale assemblage and the Porcupine group.....13

1.5 Geological characteristics of porphyry rocks.....14

1.6 Relationship between economic Au enrichment and magmatic events.....15

1.7 Chemistry and origin of felsic intrusions present in greenstone belts.....17

2.0 Analytical methods.....18

2.1 Major and trace element mapping analysis of melt inclusions in of quartz phenocrysts by LA-ICP-MS.....18

2.2 Scanning Electron Microscopy.....21

3.0 Results.....23

3.1 Petrography and mineralogy of the Paymaster, Crown, Pearl Lake porphyries and Krist fragmental unit.....23

3.1.2 Melt inclusions petrography.....27

3.2 LA-ICP-MS analyses of trace elements in melt inclusions.....29

4.0 Discussion 35

4.1 Correlation of metals……35

4.1.2 Comparison of bulk rock and melt inclusion analyses ……46

4.2 Evolution of magma and Cu-degassing in the Archean……...55

5.0 Conclusions……..59

List of Figures

Figure 1. An overview map of the district of Timmins…….12

Figure 2. Stratigraphic column illustrating the sequence of the Timmins area……..133

Figure 3. LA-ICPMS transient signal of a single melt inclusion hosted in a quartz phenocryst.. 21

Figure 4. Backscattered electron-scanning electron microscopy (BSE-SEM)……..22

Figure 5. Slab images showing Krist Fragmental and Crown porphyry hand ……23

Figure 6. Transmitted and reflected light microscopy……...24

Figure 7. Melt inclusions hosted in quartz phenocrysts……27

Figure 8. Comparison of trace element analyses of melt inclusions from the Paymaster porphyry… ……31

Figure 9. Comparison of trace element analyses of melt inclusions from Crown porphyry …….....32

Figure 10. Comparison of trace element analyses of melt inclusions from the Krist Fragmental. ……...33

Figure 11. Trace element plot of the Pearl Lake porphyry..……..34

Figure 12. Discrimination plot of granites and TAS classification diagram…….38

Figure13. Nb/Ta vs Zr/Hf diagram……..…….39

Figure 14. Comparison between the concentrations of metals from melt inclusions……41

Figure 15. Rb-Sr-Ba ternary diagram ……45

F**igure 16**. Cu-Mo-W ternary diagram……46

Figure 17. Multi figure panel illustrating the relationship of metals…….48

Figure 18. Multi figure panel illustrating the relationship of metas 49

Figure 19. Comparison of mineralized modern and ancient porphyry systems……...…54

Figure 20: Comparison between barren modern and ancient porphyry systems……...55

Figure 21: Discrimination diagram of adakities……....57

Figure 22. Sry/Y vs Nb/Ta and Sr/Y vs Cu diagram…….....…….59

1.0 Introduction

1.1 Archean lode gold deposits

The ~2400-km wide Superior Province in the south-central Canadian Shield forms the one the largest provinces within the core of the Canadian Shield and an important source of mineral wealth. In the southern part of the Superior Province, the Archean Abitibi greenstone belt (within the Abitibi sub-province) contain some of the most significant economic mineral deposits in Canada including world-class lode gold deposits in the Timmins district and volcanogenic-associated Cu-Zn-Pb massive sulphide deposits (VMS) of the Noranda camp.

Within the Abitibi greenstone belt, associated with the Porcupine-Destor fault, lies the mining district of Timmins which is home to the largest lode gold-producing district in North America. Over 110 M ounces of gold has been produced from this district, with an additional 70+ M ounces produced from deposits along the adjacent (to the south-southeast) Larder Lake-Cadillac fault. Most of the Au is hosted in quartz-carbonate vein systems within metamorphic rocks of greenschist facies (Gray and Hutchinson, 2001). Present as a minor portion of the total Au endowment of the district, and historically mined, were Cu-Mo-Au porphyry deposits hosted within felsic porphyry stocks intruding in the metamorphic rocks of the Tisdale assemblage.

The Tisdale assemblage consists of: i) a lower portion consisting of mixed ultramafics and Mg-tholeiite mafic, metavolcanics rocks that have an age of 2707 Ma and ;ii) a middle sequence dominated by Fe-tholeiitic basalts capped by two distinctive variolitic units, and ;iii) an upper sequence consisting dominantly of calc-alkaline felsic pyroclastic rocks known as the Krist fragmental unit that has an age date of 2698 Ma. These stocks are present

in vicinity to some of the world-class deposits of the district such as the Hollinger and McIntyre deposits, that show an evident spatial relationship between the rocks of the Tisdale assemblage and the porphyry stocks. A considerable amount of research has been done in the Timmins district with some focused on, or including, the porphyry rocks and the minor episodes of porphyry-style mineralization associated with them (e.g. Ferguson et al. 1968; Davies and Luhta 1978a; Pyke 1982; Burrows and Spooner 1986, 1989; Mason and Melnik 1986; Wood et al 1986; Corfu et al. 1989; Burrows et al. 1993; Brisbin 2000; Gray and Hutchinson 2001; Ayer et al. 2002a, 2002b, 2003, 2005; Bateman et al. 2004, 2005, 2008; Dinel et al. 2008). There is still some debate regarding the relationship between several key Au mineralizing events and the emplacement of the felsic porphyry intrusions.

1.2 Archean mesothermal gold deposits

Almost all of the major tectonic subdivisions of the Canadian landmass contain lode gold deposits. These deposits are dominantly hosted in terranes that contain metavolcanic and clastic metasedimentary rocks of low to medium metamorphic grade. Of these deposits, the ones that are of economic importance are found concentrated in the Archean greenstone terranes of the Superior and Slave provinces (Poulsen, 1996). In the past, there has been disagreement regarding the geological classification of lode gold deposits, mainly owing to the diversity of their host rocks.

One of the main aspects that have been important in classifying lode gold deposits is the temperature-depth concept. Lindgren (1933) divided the hydrothermal ore deposits into "thermal" types, *epithermal, mesothermal and hypothermal.* Lindgren recognized that his scheme not only applied to the genetic temperature aspect of the deposits but also the depth

aspect of the Earth's crust at which these different types of deposits form. This aspect of his classification scheme holds true currently, thus, *epithermal* gold deposits are those formed 1 to 3 km in the Earth's crust, *mesothermal* deposits form generally between 3 to 5 km, and *hypothermal* deposits form at depths of more than 5 km. The depth ranges implied for each of the three types are not firmly established but are guidelines that reflect variations in lithostatic pressure, fluid pressure, crustal temperature and metamorphic facies transitions, the availability of meteoric fluids, and the vertical extent of brittle and ductile fields of deformation and seismicity (Poulsen, 1996).

Mesothermal deposits form typically at depths of 3 to 5 kilometers below the Earth's crust, and generally at temperatures at or above 350°C. Quartz-carbonate vein Au deposits are a subtype of mesothermal Au deposits (Dubé and Gosselin, 2007; Robert 1996). For decades, the origin of quartz-carbonate vein deposits has been debated and one of the main controversies of this type of deposit is the fluid source (Dubé and Gosselin, 2007). Ore fluid typically deposits Au at 1.5 ± 0.5 kb and 350° ± 50°C. gold is transported as a reduced sulphur complex (Groves et al., 2003)

There have been different proposals regarding the origin of heat and magmatic fluids in this type of deposit which include: (i) a mantle related model, (ii) a magmatic source of fluids, and (iii) deep convection of heat and the fluid for the source of magmatic fluids (MacInnis, 2010). Spooner (1991) introduced a genetic model proposing a magmatic origin for Archean Au-quartz vein systems. It was suggested by him that the Au enrichment was a result of partitioning of ore minerals into fluid from silicate melt which contained a certain amount of dissolved H_2O-CO_2-NaCl, and transportation of ore minerals in the exsolved

solution with or without fluid mixing, followed by subsequent Au deposition (Spooner, 1991). This model proposed by Spooner (1991) applied to porphyry Cu-Au deposits, Au mineralization in intrusion-centered systems, Au skarns and their close spatial relationship. However, a major limitation of this model is the lack of, or ambiguity of the evidence that directly implicates a magmatic fluid source aside from intrusion-ore spatial relationships. Consequently, metamorphic models have prevailed for mesothermal gold (Goldfarb et al., 2005).

Another genetic model was proposed by Spooner (1992) which described a possible relationship between Archean Au quartz veins and epithermal Au-Ag, Au skarn and Cordilleran Au quartz vein hydrothermal ore systems. This relationship between the four deposit styles was based on a common signature of chalcophile/siderophile element assemblage enrichment and led Spooner (1992) to suggest that ore fluids were derived from, and/or enriched in metals by, the dissolution of magmatic sulphide liquid droplets by high-temperature magmatic vapour. Spooner (1992) further suggested that due to high partition coefficients associated with fluid exsolution, high aqueous-phase solubility of the sulphide component at high temperatures and selective Au precipitation relative to other ore minerals, chalcophile element scavenging by fluids occurred and is a key component of the enrichment process.

The spatial relationship between these porphyry rocks and the largest gold deposits in the Timmins district invoked substantial discussion regarding the genetic relationship between porphyry emplacement and ore formation. As it stands, modern and ancient porphyry systems have many geochemical similarities, but the lack of data for Archean porphyry systems leaves an uncertainty regarding the question; are modern and ancient porphyry

systems analogous? It is the aim of this thesis to provide a better understanding of the relationship of the porphyries with the gold mineralization events at Timmins, and to evaluate the use of melt inclusions in characterizing magmatic processes in Archean porphyry systems in general.

1.3 Regional geological setting of Timmins, Ontario

The Abitibi greenstone belt is a 750-km-long by 200-km-wide belt, comprised of intrusive, coeval metamorphosed, subvolcanic rocks, and locally derived clastic and chemically sedimentary rocks, and granitoid batholiths (Gray and Hutchinson, 2001). Lying within the Abitibi sub-province of the Archean Superior craton is the Timmins-Porcupine gold camp along the northern margin of the Destor-Porcupine fault. The Destor-Porcupine fault is a major east-west fault zone that extends from Timmins, Ontario, to the Noranda area in Quebec (Wilson 1949; Dimroth et al. 1973; Gelinas et al. 1977). This deformation zone along with the Larder Lake-Cadillac deformation zone are very significant within the Abitibi sub-province in terms of gold production. The Destor-Porcupine fault extended much further in the Early Precambrian as it is cut off at either end by younger fault zones.

Many intrusions across the Superior Province have ages similar to their metavolcanic counterparts. (Corfu and Andrews 1987) dated post-volcanic intrusions yielding ages between 2720 and 2700 Ma in the northwestern greenstone terranes. An albitite dike that dates 2673 Ma (Marmont and Corfu 1989) is the youngest intrusion in the Timmins district. The geochronological data demonstrated by (Corfu and Stott 1986, Corfu and Grunsky

1987, Marmont and Corfu 1989; Corfu et al. 1989) specifies that in the greenstone belts across the Superior Province, the latest volcanic activity occurred at different times. In the northwestern greenstone belts, the final volcanic activity is older (>2900 to 2720 Ma) than in the southeastern green stone belts (>2900 to 2700 Ma).

Separated by the Destor-Porcupine fault are two main structural domains: the area north of the fault which encompasses the main gold mining camp, and the area south of the fault. The Timmins gold camp is comprised of discrete supracrustal units, four of which are identified as the Deloro, Tisdale, Porcupine and Timiskaming assemblages (Fig.2). The Keewatin series is comprised of the older Deloro Group and a younger Tisdale assemblage (Dunbar, 1984). The 4.5 km thick Deloro group is of calc-alkalic composition, consisting mainly basaltic and andesitic flows in the lower apart with dacitic flows and dacitic-rhyolitic pyroclastic flows towards the top of the sequence (Pyke, 1982; Wood et al.,1986). The Tisdale assemblage hosts the Krist fragmental rocks, Pearl Lake porphyry, Crown porphyry and Paymaster porphyry, which are the focus of this thesis, and is described below (Fig. 3)

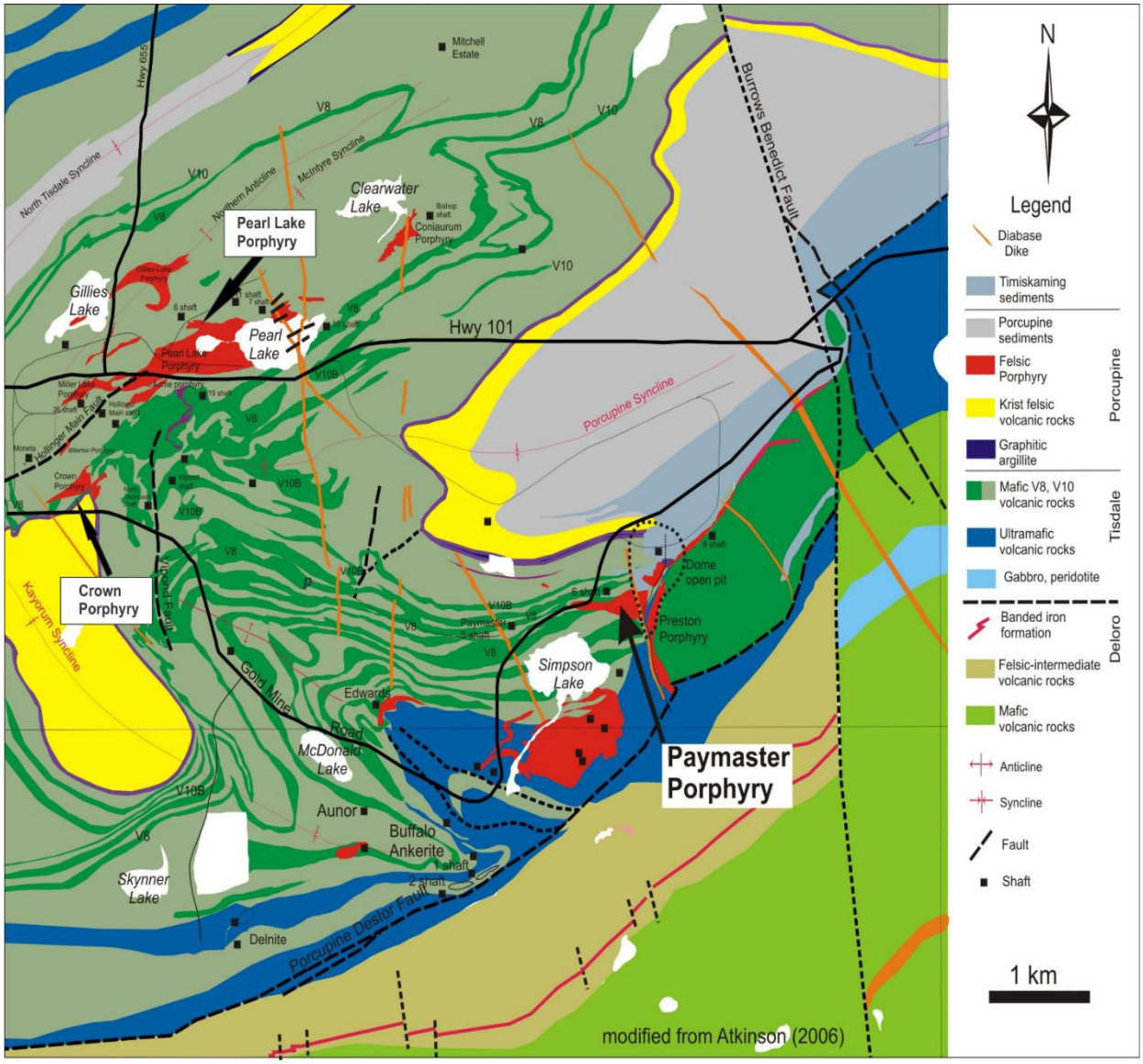

Figure 1. An overview map of the Timmins District showing the localities of the Paymaster Porphyry, Pearl Lake Porphyry, Crown Porphyry and the Krist fragmental rocks. The map was modified from McInnis (2010) and Atkinson (2006).

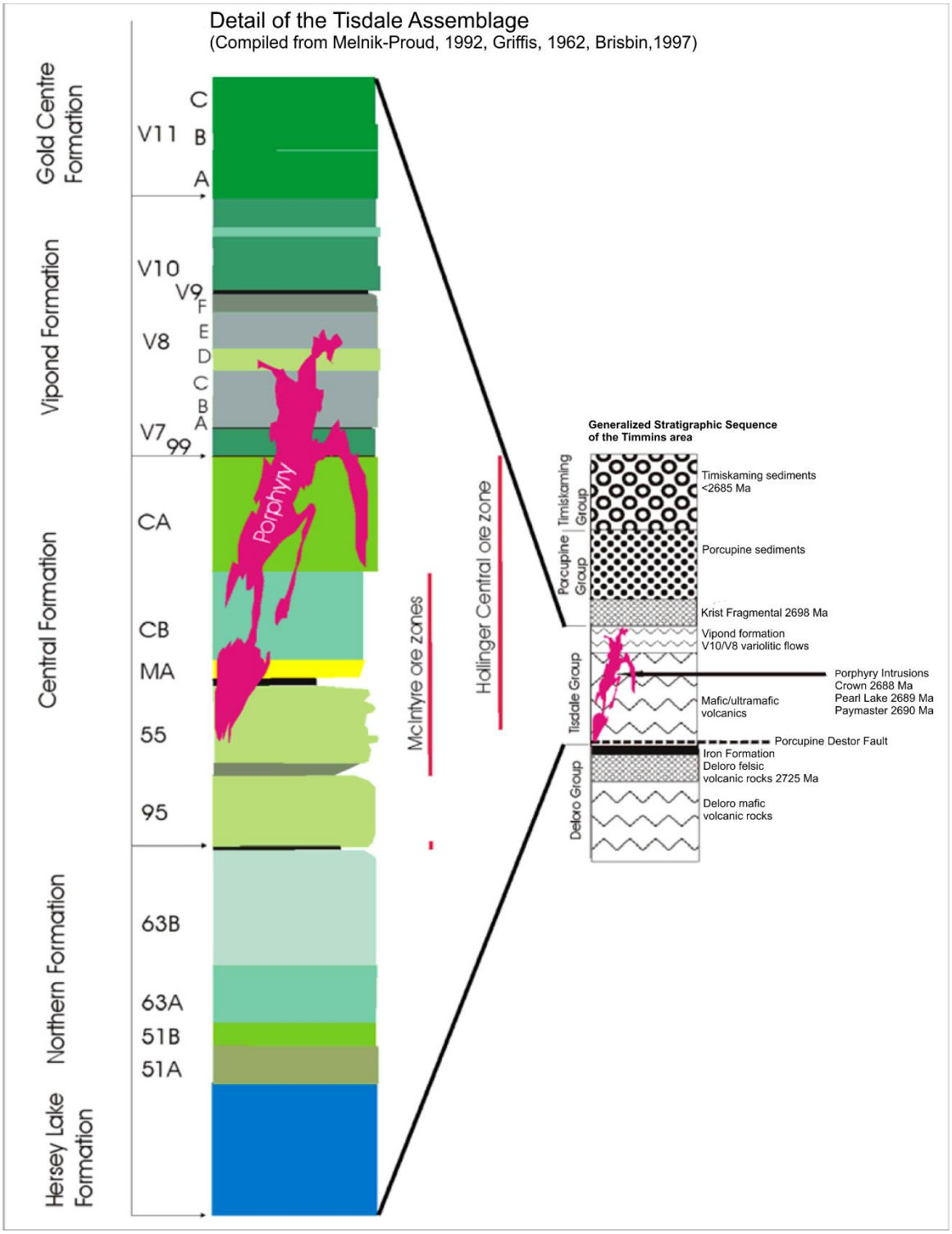

Figure 2. Stratigraphic column illustrating the sequence of the Timmins area, compiled from Melnick-Proud, (1992), Griffis (1962), and Brisbin (1997). Modified from Atkinson, (2007)

1.4 Tisdale assemblage and the Porcupine group

The 3500m Tisdale assemblage which was previously referred to as the Tisdale group is made up of five different formations (Dunbar, 1948, Jones, 1948; Ferguson et al., 1968), two of which, the Central and Vipond Formations are significant contributors to hosting most economic deposits. The Tisdale assemblage is underlain by Mg rich tholeiitic volcanic rocks and basaltic komatiites and is overlain by calc-alkaline volcaniclastic and or pyroclastic dacitic rocks (Pyke, 1982). The Krist Fragmental assemblage is found at the base of the Porcupine assemblage and is calc-alkalic at the top of the unit with felsic volcaniclastic rocks, and consists of carbonaceous argillite at the base. A second bed of carbonaceous argillite is present within the Krist formation, marking a hiatus period in volcanism, indicating that the volcaniclastic rocks were emplaced in two eruptive periods (Pressacco, 1999). The felsic volcaniclastic units have in abundance lapilli tuff and lapillistone, which contain a variety of fragment composition that are dominated by feldspar-porphyritic tuffs and felsic flows (Pressacco, 1999). The Krist Fragmental assemblage fills structural basins (Porcupine and Kayorum Syncline) to an approximate thickness of 200 meters (Fig. A1: Brisbin 2000). The Porcupine and Kayorum syncline exposures of the Krist assemblage consists rounded pyroclastic felsic volcanic rocks that contain sub-rounded to rounded porphyry fragments up to a few centimeters in size (Fig. 6), with the matrix containing small quartz phenocrysts and alteration minerals including white mica and chlorite (MacDonald, 2010). Alteration of the felsic volcanic rocks includes weak to moderately developed sericite-carbonate that affected the felsdpathic portion of the

matrix, resulting in a cloudy brownish-grey appearance of feldspars in thin section (MacDonald 2010)

1.5 Geological characteristics of the porphyry rocks

Two distinct varieties of porphyry were identified; quartz-feldspar porphyry and feldspar porphyry. Both are silica-saturated, variably quartz and feldspar porphyritic, lacking in potassium feldspar and of porphyritic texture. Although similar in whole-rock composition, the two porphyries have distinctly different accessory mineral assemblages along with trace element geochemical signatures (Gray and Hutchinson, 2001). Petrographically, quartz-feldspar porphyry is different from feldspar porphyry, however in hand specimens and outcrops, due to the effects of low grade metamorphism and hydrothermal alteration, the differences are not always readily distinguishable.

The following petrographic descriptions are from Gray and Hutchinson (2001). Quartz-feldspar porphyry has a ground mass of 50 vol% and is dominated by quartz phenocrysts (5-30%) and oligoclase phenocrysts (70-95%) and average modes are about 10 percent quartz and 90 percent oligoclase. Quartz phenocrysts are rounded, subhedral and equant, 100-4000µm in diameter. Oligoclase forms anhedral to euhedral equant grains and laths 200 to 4000µm in diameter and length. Feldspar porphyry is 45 vol% groundmass and is dominated by oligoclase (>99%) and minor quartz. Quartz phenocrysts are rounded, subhedral, equant grains 100-3000µm in diameter whereas the oligoclase phenocrysts are subhedral to euhedral and 200-4000µm in diameter (Gray and Hutchinson, 2001). As illustrated in the stratigraphy column of the Tisdale assemblage (Fig. 3) and from various sources (Ferguson et al. 1968, Pyke 1982, Dinel et al. 2008, MacDonald 2010), the Krist

fragmetal unit is known to predate the porphyries by ~ 6 to 10 Ma but contains porphyry fragments.

1.6 Relationship between economic Au and magmatic events

Over 50 mines have produced almost 70 M oz of total gold in the Timmins District (Dome mine, Hollinger-McIntrye mine, Paymaster mine, Pamour mine, Red Lake mine, Hoyle Pond mine), out of which about 80% has been in the vicinity of or within felsic porphyritic rocks. It is believed amongst some researchers that the intrusive activity of felsic porphyry rocks is younger than the Au zones found within the district, which has led to the interpretation that the Timmins District contains Archean lode gold deposits that formed synonymous to structural deformation (Burrows and Spooner, 1993). Other researchers believe that the Au is formed from hydrothermal activity related to the development of albitite dikes which frequently intrude felsic porphyries, while some link the development to a porphyry-type hydrothermal system (Mason and Melnik, 1986).

Gray and Hutchinson (2001) recognized that there were multiple, successive stages of gold deposition in the Porcupine camp. The metasedimentary rocks of the Porcupine assemblage lie conformably upon the felsic metavolcanics rocks at the top of the Tisdale assemblage and because of this relationship between the Porcupine and Tisdale assemblage (Pyke 1982) argued that the Porcupine assemblage was temporally coeval with the entirety of the Tisdale assemblage. Gray and Hutchinson (2001), recognized auriferous clasts in the basal Timiskaming conglomerate, clearly derived from the older, underlying rocks, proving the existence of pre-Timiskaming gold enrichment.

Two differing types of epigenetic gold deposition are recognized at the Dome mine. Copper-Au and Mo were deposited during an event that accompanied emplacement of the Paymaster porphyry intrusion. These intrusions are cut and overprinted by late planar, sheeted and en-echelon auriferous quartz veins and by mineralized fault zones (Gray and Hutchinson 2001). Copper-Au and Mo mineralization is also present in the Pearl Lake porphyry (Davies and Luhta, 1978) and the Coniaurum porphyry, with the latter merging with the main mass of the Pearl Lake porphyry at depth (Ferguson et al., 1968, Piroshco and Hodgson, 1988). Differing textures and mineral composition in these auriferous veins further indicate multiple stages of vein formation, postdating all emplacement of the felsic porphyry intrusions (Gray and Hutchinson 2001). With the aid of isotopic dating, the age of the Cu-Au-Mo mineralizing event from the study of Gray and Hutchinson (2001) was 2688 ± 2 Ma. A maximum age for the mesothermal gold deposition in the area is that of an albitite dike, dated at 2673 ± 6 Ma (Corfu et al., 1989) that is cut by auriferous quartz-carbonate veins at the McIntyre mine. Rhenium-Os age dating of molybdenite from both the McIntryre and Dome ore systems yielded ages of 2670-2672 Ma (Ayer et al. 2003; Bateman et al. 2004). Collectively, these observations indicate multiple periods of Au emplacement into supracrustal rocks, associated with distinctly different geologic events occurring over a span of 7 Ma, and possibly as much as 19 Ma (Gray and Hutchinson 2001). Gray and Hutchinson (2001) showed in their study that although some Au was deposited during a Cu-Au-Mo event temporally linked to porphyry emplacement, the vast majority of the Au in Timmins was emplaced significantly later (~15 Ma) than the porphyries. The documentation of at least three broad periods of gold emplacement, at least two of which are pre-metamorphic, is permissive and supportive of a genetic hypothesis that invokes

metamorphogenic remobilization of Au from earlier formed deposits of unknown origin. (Gray and Hutchinson, 2001).

1.7 Chemistry and origin of felsic intrusions present in greenstone belts

Greenstone belts comprise of volcaniclastics, granitoids and clastic/chemical sediments derived from continental, trench, oceanic and arc material, and usually show low-grade metamorphic assemblages which normally contain actinolite, epidote, chlorite and albite (Winters, 2001). Many researchers strongly debate the relevance of plume magmatism, rifting and subduction to the formation of Archean greenstone belts (Tomlinson, 2004) and the overall accordance amongst researchers is that the tectonically active mantle would have been losing heat at the ocean ridges. It is believed that mantle convection which occurred at that time was very intense and the production and recycling of tholeiitic and komatiitic magmas was rapid (Winter, 2001).

As a result of shallow dipping subduction zones which were a result of the subduction of warm crust, subduction zones with high geotherms resulted in significant melting of the subducted slab (Tomlinson, 2004). The diversity of greenstone belt sequences required a wide variety of tectono-magmatic processes to create them, to do this the most likely processes would have been the process of plate tectonics during the Archean (Tomlinson, 2004).

It is suggested that greenstone belts in the Superior Province were derived from diverse arc environments (oceanic island arc, back arc, and primitive island arc; Tomlinson, 2004). Greenstone belts tend to show continental rock sequences that appear to indicate convergent and divergent plate settings which are related to subduction zone magmatism

as well as rifting. Continental orogenic granitoids such as those common to greenstone belts are thought to develop by mature arcs merging together to form continental arcs and continents (Tomlinson, 2004). A two-step melting process in the mantle wedge is used as a model for continental arc formation. the first step produces basaltic magma solely from the mantle source (Tomlinson, 2004). Initially, a basaltic magma is produced solely from the mantle source. The magma pools at the bottom of the less dense crust where partial melting occurs via mafic underplating, which is followed by a resulting tonalitic magma to rise as it is light enough, to a shallow level and evolve further by fractionation before solidification occurs (Tomlinson, 2004). These sequences described by Tomlinson (2004) comprise the Superior Province and are submarine volcanic plains, diverse volcanic sequences, submerged continental platforms and continental felsic volcanic centers.

2.0 Analytical methods

The samples studied are from the Paymaster Porphyry, the Crown Porphyry, the Pearl Lake Porphyry and the Krist fragmental unit. Thick sections were made for melt inclusion analysis from these units, with 4 thick sections for the Paymaster, 3 thick sections for the Krist fragmental, and 4 thick sections for the Crown prepared. Quartz phenocrysts from all the thick sections were mapped under an Olympus BX-53 microscope equipped with Qimaging digital camera.

2.1 Major and trace element mapping of quartz phenocrysts by Laser Ablation Inductively Coupled Mass Spectrometry (LA-ICP-MS)

The composition of the melt inclusions was determined at the Magmatic and Ore-Forming Processes Research Laboratory at the University of Toronto. An NWR 193UC ArF Excimer laser ablation system attached to an Agilent 7900 quadrupole mass spectrometer

was used. The instrument was tuned to maximize sensitivity while maintaining robust plasma conditions (U≈Th on NBS SRM610) and low oxide and doubly charge ion production rates (ThO/Th < 0.3%; Mass21/^{42}Ca < 0.3%). Helium was used as a carrier gas at a flow rate of 1.0 l/min. The NBS SRM610 silicate glass standard was used for the quantification of element concentration ratios. The analyses of 16 unknowns were bracketed by 2 standard analyses at the beginning and the end of each analysis block. The dwell times of 49 major and trace elements was set to 10 ms, with the exceptions of Cu set to 20 ms and Mo set to 30 ms respectively. The method of Halter et al. (2002) was used to quantify the inclusions, i.e. the entire unhomogenized inclusions were ablated along with some host quartz. The melt inclusion compositions were quantified using the software SILLS (Guillong et al., 2008), and integrated signal intensities were corrected for the background and host signal. Al_2O_3 was used as an internal standard with its value set to 19.63%. This value was based on the value determined by MacInnis (2010).

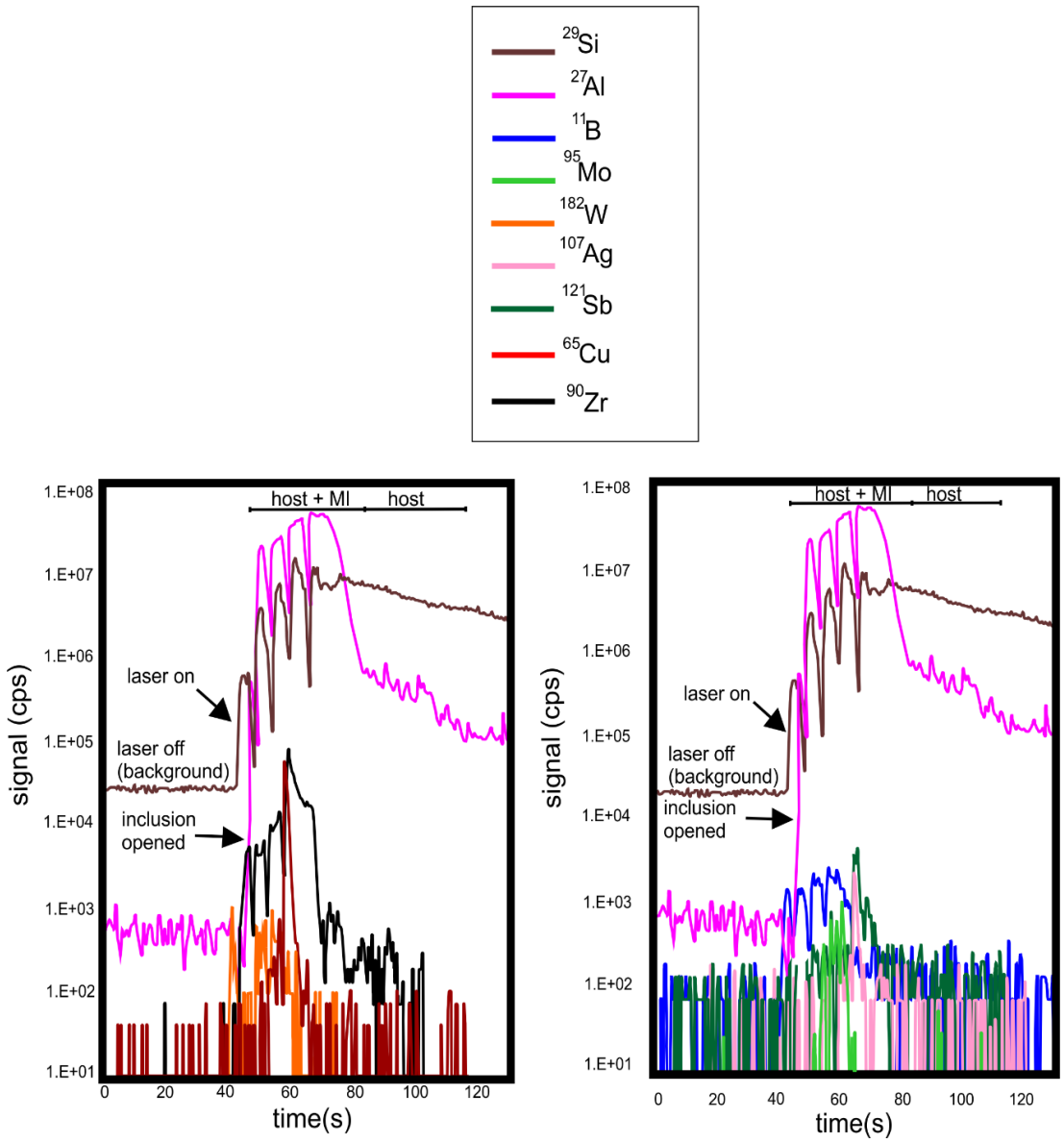

Figure 3 LA-ICPMS transient signal of a single melt inclusion hosted in a quartz phenocryst. Spectra shows signal intensity (counts per second) vs time for a variety of measured isotopes to be quantified.

2.2 Scanning Electron Microscopy (SEM)

Images and quantitative analyses of two mineralized samples were obtained. The first sample was a thick section comprised of a mineralized pyrite-chalcopyrite-gold hosted in the Pearl Lake porphyry, and the second sample was a small piece of the Pearl Lake porphyry containing some molybdenite. The data was obtained using a TESCAN MIRA3 LMU FESEM, at Saint Mary's University equipped with an Oxford Instrument INCA X-max 80mm^2 silicon drift detector (SDD) energy dispersive system (EDS) detector linked to a desktop PC (INCA software – published by ETAS).

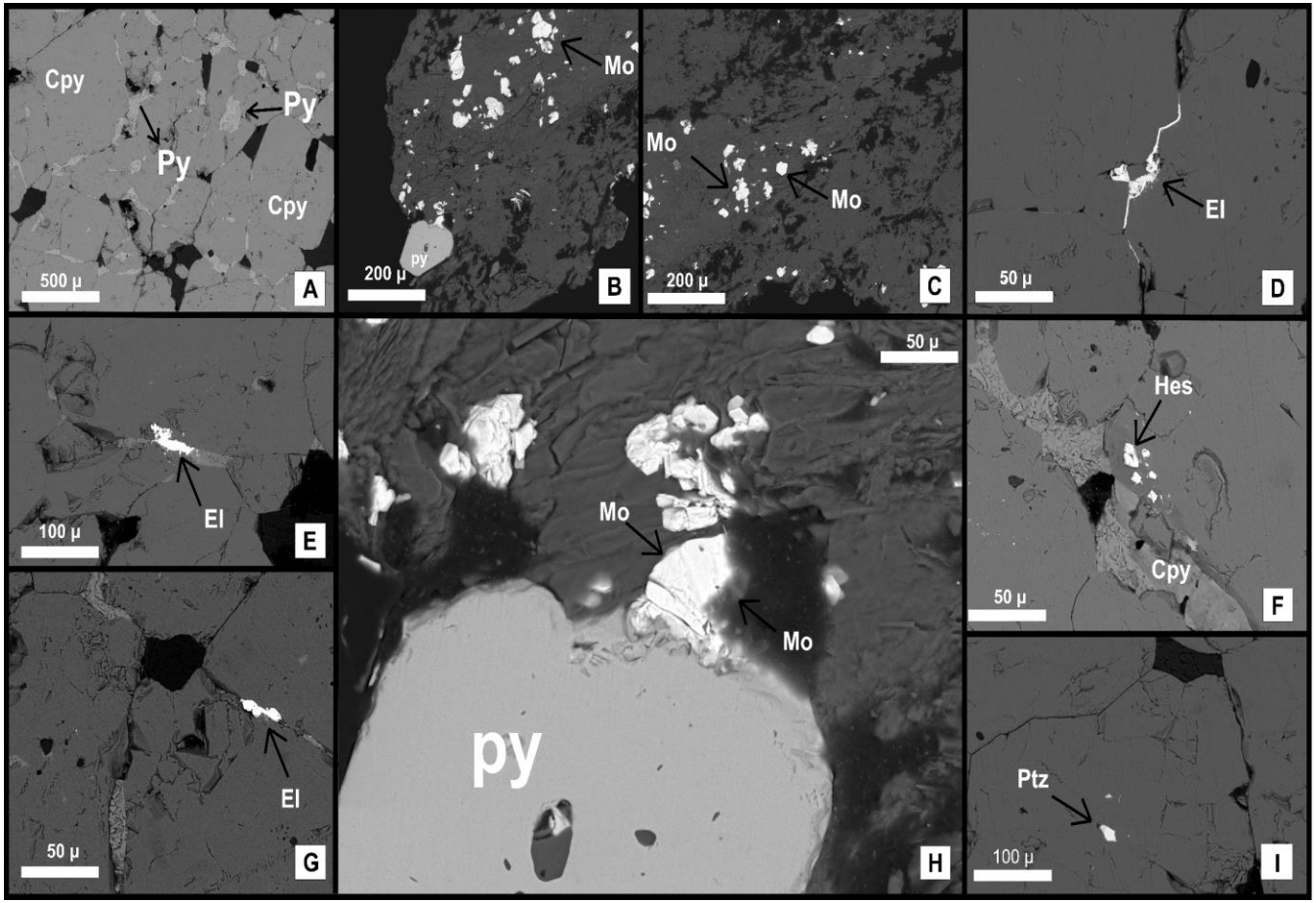

Figure 4. Backscattered electron-scanning electron microscopy (BSE-SEM) images showing (A) Chalcopyrite (Cpy) grain boundary hosted pyrite. (B, C) Irregularly shaped molybdenite (Mo) dispersed along with some pyrite showing blebby texture. (D) Electrum (El) infilling cracks in a a grain of pyrite (Py). (E) Hessite (Hes) filling up the cracks of a pyrite grain. (F) inclusions filled by Hess along with some visible Py. (G) Fracture being infilled by (El). (H) Close-up of the area showed in images (B, C). (I) Inclusion of petzite (Ptz) in a grain of pyrite.

3.0Results

3.1 Petrography of the porphyry rocks and Krist fragmental

The Krist fragmental shows mixture of a lighter coloured matrix which is composed of clasts that are fragments of the porphyritic rock (Fig. 5). Quartz phenocrysts (circled) in images c and d were the host of melt inclusions. The Krist fragmental rocks are matrix supported, containing fragments of relatively fresh porphyry. It is observed that the porphyry rocks are undergoing fragmentation and chemical changes as shown by the clast in image (B), as it is evident that there is a fresh porphyry fragment with a dark matrix but there is also another fragment in that same sample that appear as though it has been re-equilibrated with the matrix.

The Paymaster, Pearl Lake, and Crown porphyries contained abundant amounts of quartz, plagioclase (var. oligoclase), potassium feldspar, and calcite which ranged 5%. Biotite and pyrite are present in each site ranging from 1-4 vol% in abundance. A small amount of rutile (~1%) was found rimming pyrite crystals (Fig. 6). Apatite and zircon were reportedly found within these sites in trace amounts by MacInnis (2010). Paymaster also contained a trace amounts of baddelyite and garnet (MacInnis 2010). Early and late generations of plagioclase were found at Paymaster and Crown Lake, while quartz was found to have early and late generations within the Pearl Lake porphyry (MacInnis, 2010). All four of these sites are very similar with respect to their mineralogy and mineral abundances. The minerals listed from most abundant to least abundant that are found at all four sites are: quartz (~25-35%), plagioclase (~20-40%), potassium feldspar (~15-20%), calcite (~10%), and muscovite (~10-20%). Common trace minerals found were apatite and zircon (MacInnis, 2010).

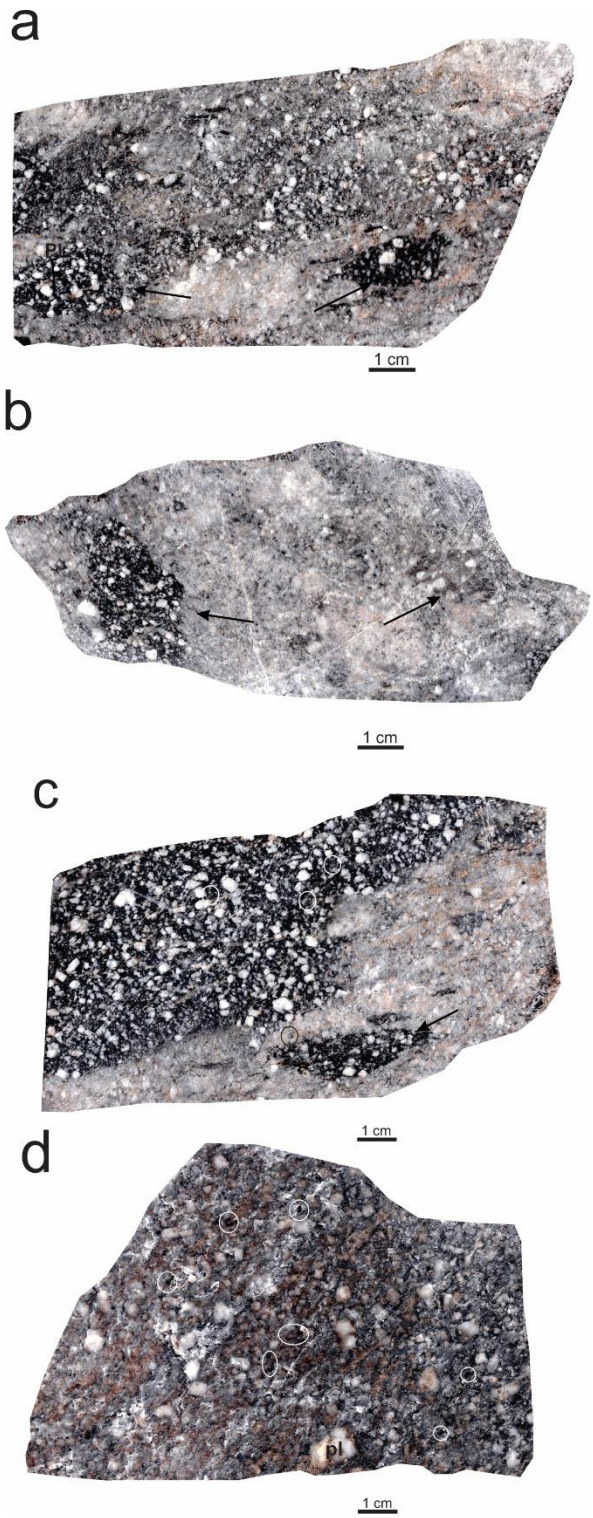

Figure 5. Slab images showing (a) Krist fragmental hand sample with inclusions of porphyry clasts and plagioclase phenocrysts (b) Krist sample with more porphyry clast. (c) Krist sample showing quartz phenocrysts (circled) along with a porphyry clast (d) Crown porphyry sample with visible plagioclase (bottom center) and quarts phenocrysts (circled).

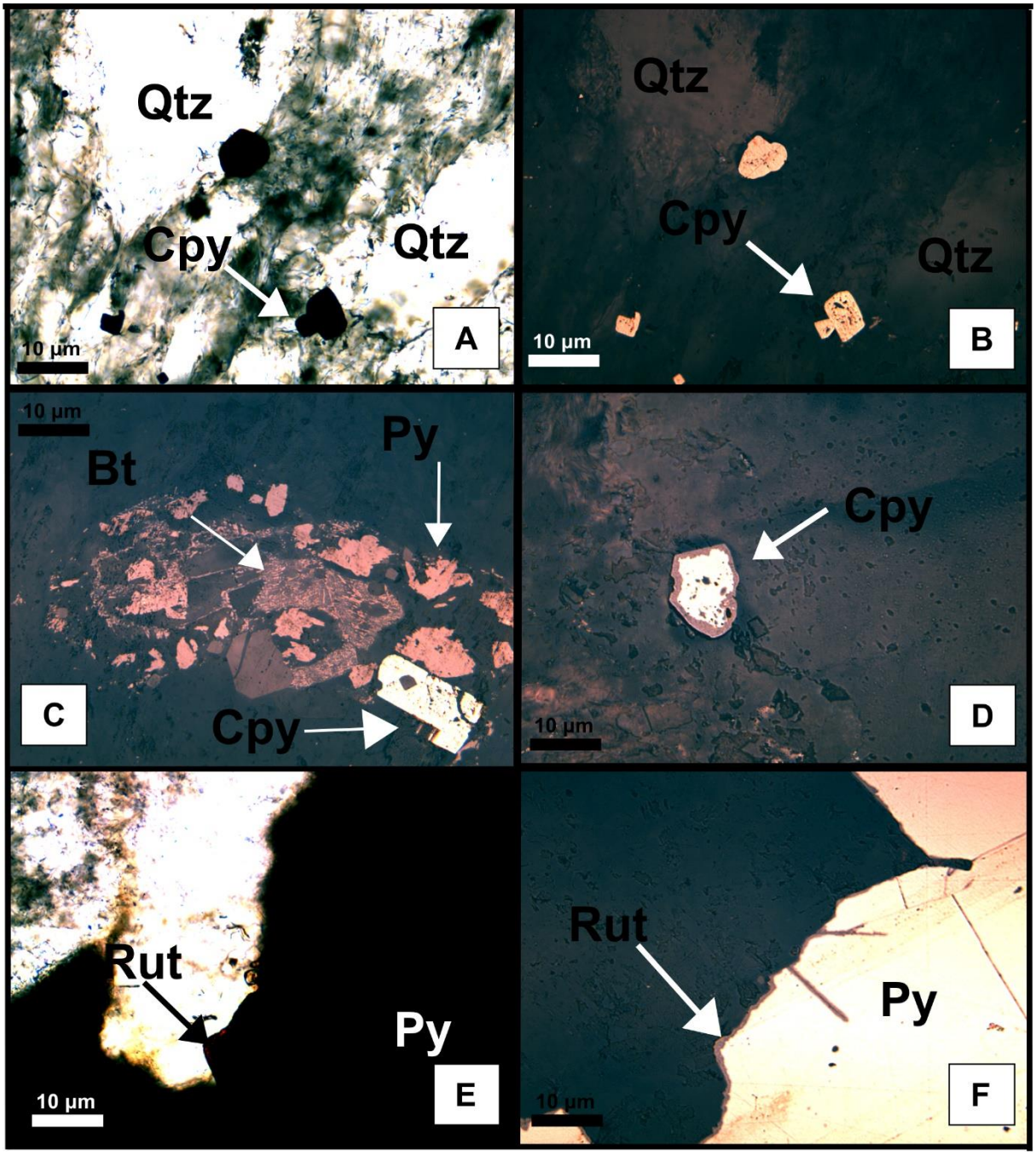

Figure 6. A) Quartz (qtz) and chalcopyrite (cpy) phenocrysts in a thin section of the paymaster porphyry under ppl (B) Same image as (A) under reflected light. (C) (cpy) along with pyrite (py) and biotite (bt) as seen with reflected light in a thin section of the crown porphyry. (D) Cpy phenocryst in the Crown porphyry. (E) Py phenocryst being rimmed by rutile = rut in a thin section of the Krist fragmental unite as seen with transmitted light and (F) as seen with reflected light.

3.1.1 Porphyry Cu-Au-Mo mineralization in Timmins

Copper-Mo-Au mineralization in the Pearl Lake porphyry of the TIS (Timmins intrusive porphyry suite) (Davies and Luhta, 1978; Mason and Melnik 1968a 1968b; Wood et al. 1986; Burrows et al. 1993; Richards and Kerrich 2007), in the Bristol Township porphyry of the TIS and the Carr Township porphyry of the CIS (Carr intrusive porphyry suite) have similarities to younger porphyry copper systems including their host rock chemistry (intermediate to felsic), host rock textures (porphyritic), the presence of potassic alteration halos surrounding a central ore zone, sulphide mineralogy (chalcopyrite ± bornite), sulphide occurrence (disseminated, clustered and stringers) and the presence of mineralized "vent breccias" textures (MacDonald, 2010). Furthermore, the rocks are geochemically similar to adakite-like rocks in the case of the TIS, for which comparables have been documented to be hosts for Phanerozoic porphyry mineralization (Oyarzun et al. 2001).

Anomalous gold (5 ppb) is associated with all of the intrusive suites. Sericite and carbonate alteration in the intrusions is largely present in the vicinity of large tonnage gold mineralization (Hollinger, MicIntyre and Dome deposits) and moderately intense ankerite-sericite alteration is the dominant alteration in the vicinity of smaller deposits (Paymaster 2-3, Buffalo Ankerite, Holmer, and Aquarius deposits, MacDonald 2010). Anomalous Cu (>1000 ppm) is associated with hematite alteration in the larger intrusions (Pearl Lake porphyry/TIS – main, Bristol Township porphyry and the Carr Township porphyry [CIS] (MacDonald 2010).

3.1.2 Melt inclusion petrography

Melt inclusions hosted in quartz phenocrsysts of the Paymaster and Crown porphyries and the Krist fragmental unit were selected that ranged from 10 microns to 25 microns in width and 10 microns to 90 microns in depth, with the average depth being 30 microns. The melt inclusions were mainly round, had a dark, cloudy appearance and were recrystallized containing a variety of solid phases such as quartz, micas and feldspars. Most of the melt inclusions were split down the middle in terms of their occurrence, with roughly half of them occurring in clusters (Fig. 7 C- D) and the other half occurring in small trails (Fig.7), with only a minority of inclusions occurring solitarily (Fig. 7 A)

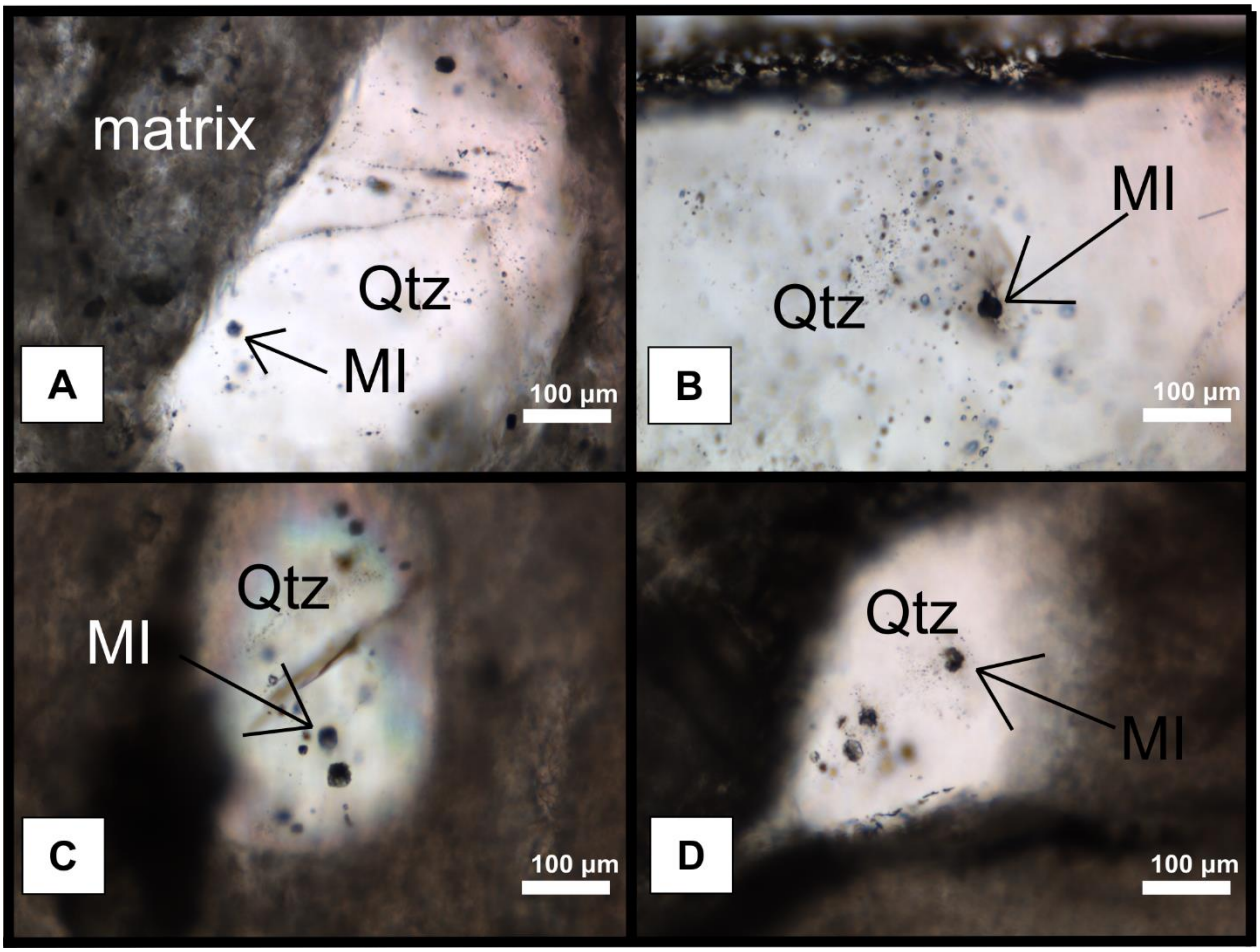

Figure 7. Melt inclusions (MI) hosted in quartz phenocrysts of (A) Paymaster Porphyry (B) Paymaster Porphyry (C) Krist Fragmental (D) Crown Porphyry

3.2 LA-ICP-MS analyses of trace elements in melt inclusions

The bulk rock trace element analyses of Paymaster and Crown Lake porphyries obtained by MacInnis (2010) were compared to the trace element concentrations in melt inclusions in quartz phenocrysts of the Paymaster and Crown Lake porphyries. For the purpose of plotting spider diagrams, all trace element data was normalized to primitive mantle abundances based on normalization values from Palme & O'Neil 2004 listed on the Geochemical Earth Reference Model (GERM) website.

A comparison of melt inclusion compositions showed strong similarities between all sites examined. The general patterns from left to right for the three localities is strikingly similar with a few differences (Figs. 8-10). At paymaster, bulk rock analyses show positive anomaly for Zr and Hf, whereas the Crown Lake porphyry does not show this shows a steady pattern (Fig. 8 - 9). LA-ICP-MS trace element analyses of melt inclusions for the Paymaster porphyry are very similar to the bulk rock data, (Fig. 8). However, the bulk rock analyses show a stronger positive anomaly for Zr and Hf as compared to the melt inclusion data, which is shows a generally negative anomaly. For the Crown Lake porphyry, the Zr and Hf concentrations in the melt inclusion analyses show a slightly positive anomaly as compared to the bulk rock analysis, which shows a steady pattern from left to right (Fig. 9). Melt inclusion analyses from a porphyry fragment in the Krist fragmental unit show a Zr and Hf pattern which resembles that of the Crown Lake porphyry (Fig. 11 - 12). The melts are depleted in Zr and Hf relative to the bulk rock (Fig. 9). The melt inclusion analyses also reveal that the metals Sc, V, Cr, Co and Ni are depleted in the Paymaster and Crown Lake porphyry as compared to the bulk rock analyses of the two localities (Fig. 8 - 9).

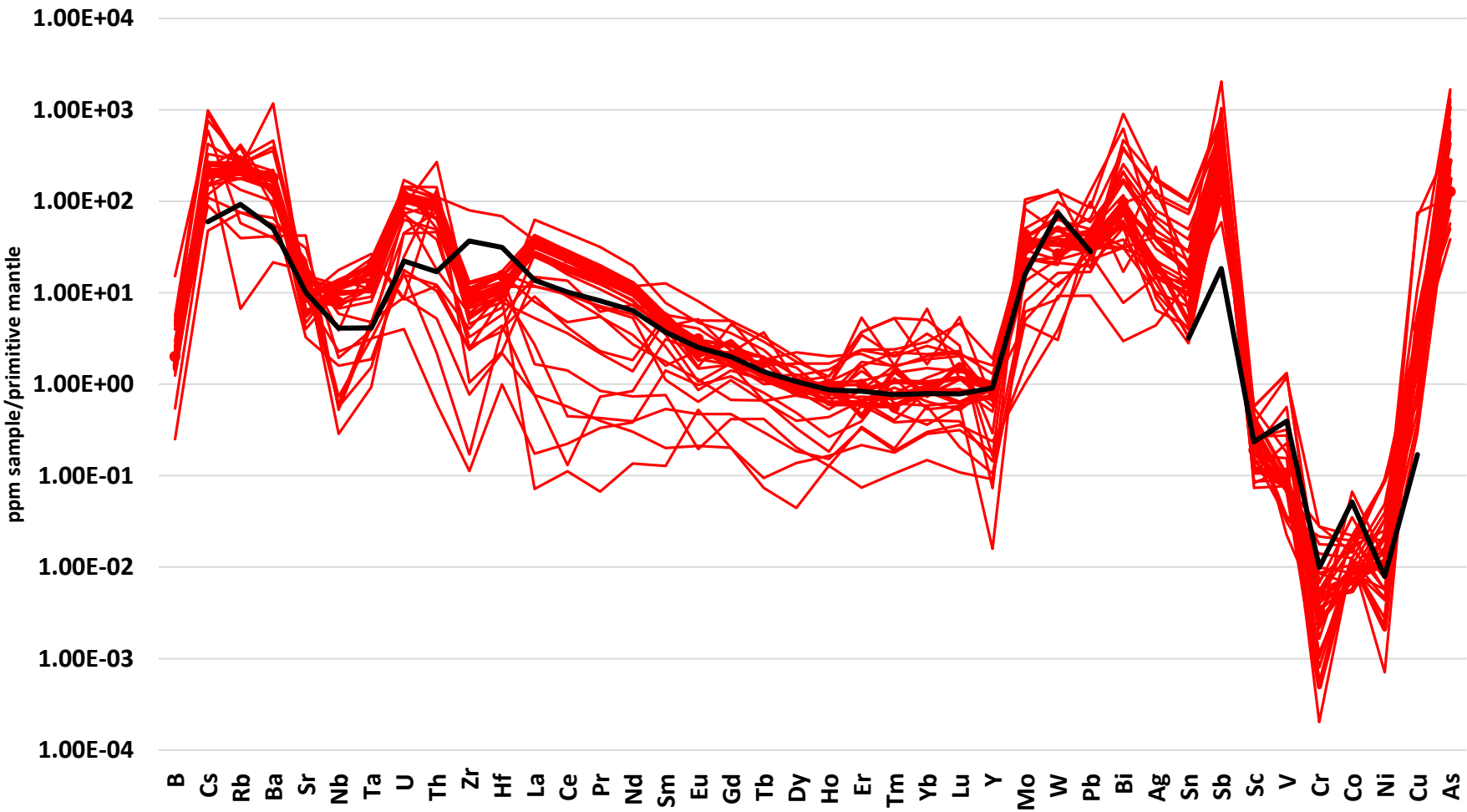

Figure 8. Comparison of trace element compositions for melt inclusions from the Paymaster porphyry and a bulk rock analysis of the Paymaster porphyry. The red lines represent the normalized LA-ICP-MS melt inclusion data patterns. The black line represents the normalized bulk rock analysis of Paymaster porphyry.

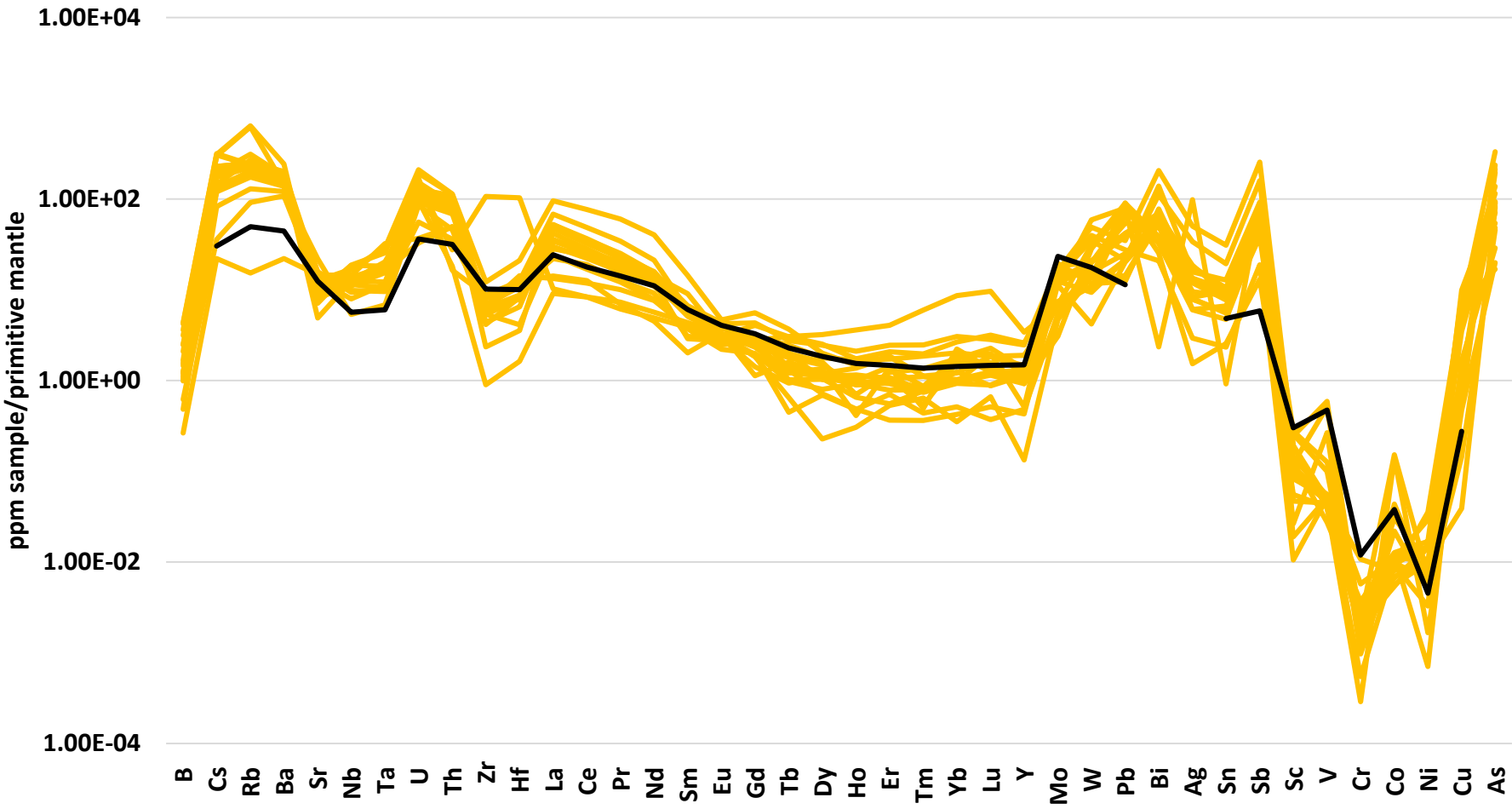

Figure 9. . Comparison of trace element compositions for melt inclusions from the Crown porphyry and a bulk rock analysis of the Crown porphyry. The yellow lines represent the normalized LA-ICP-MS melt inclusion data patterns. The black line represents the normalized bulk rock analysis of Crown porphyry.

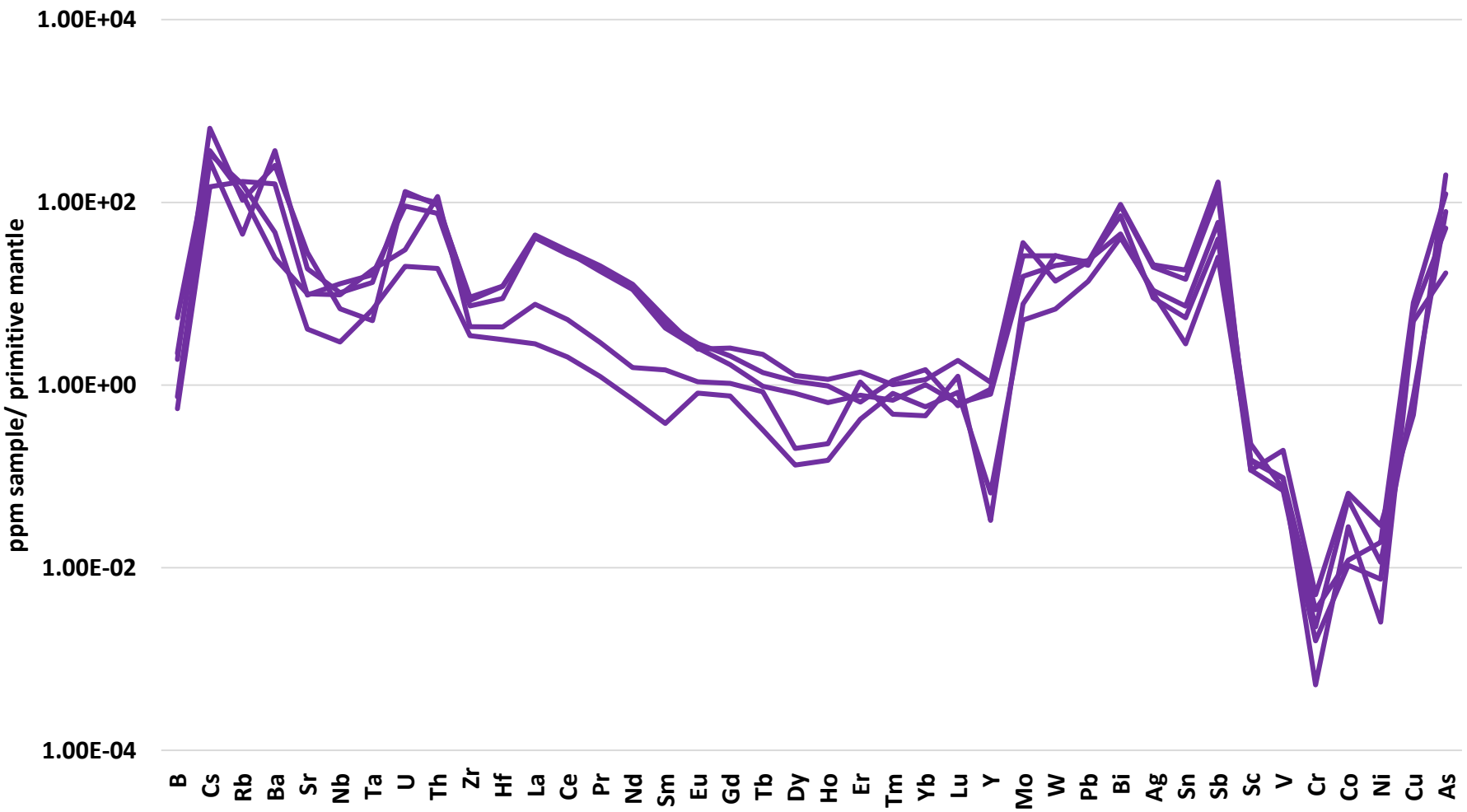

Figure 10. Trace element plot of the Krist fragmental unit. The purple lines display the trace element concentrations in melt inclusions obtained by LA-ICP-MS. Bulk rock analysis for the Krist fragmental unit was not obtained.

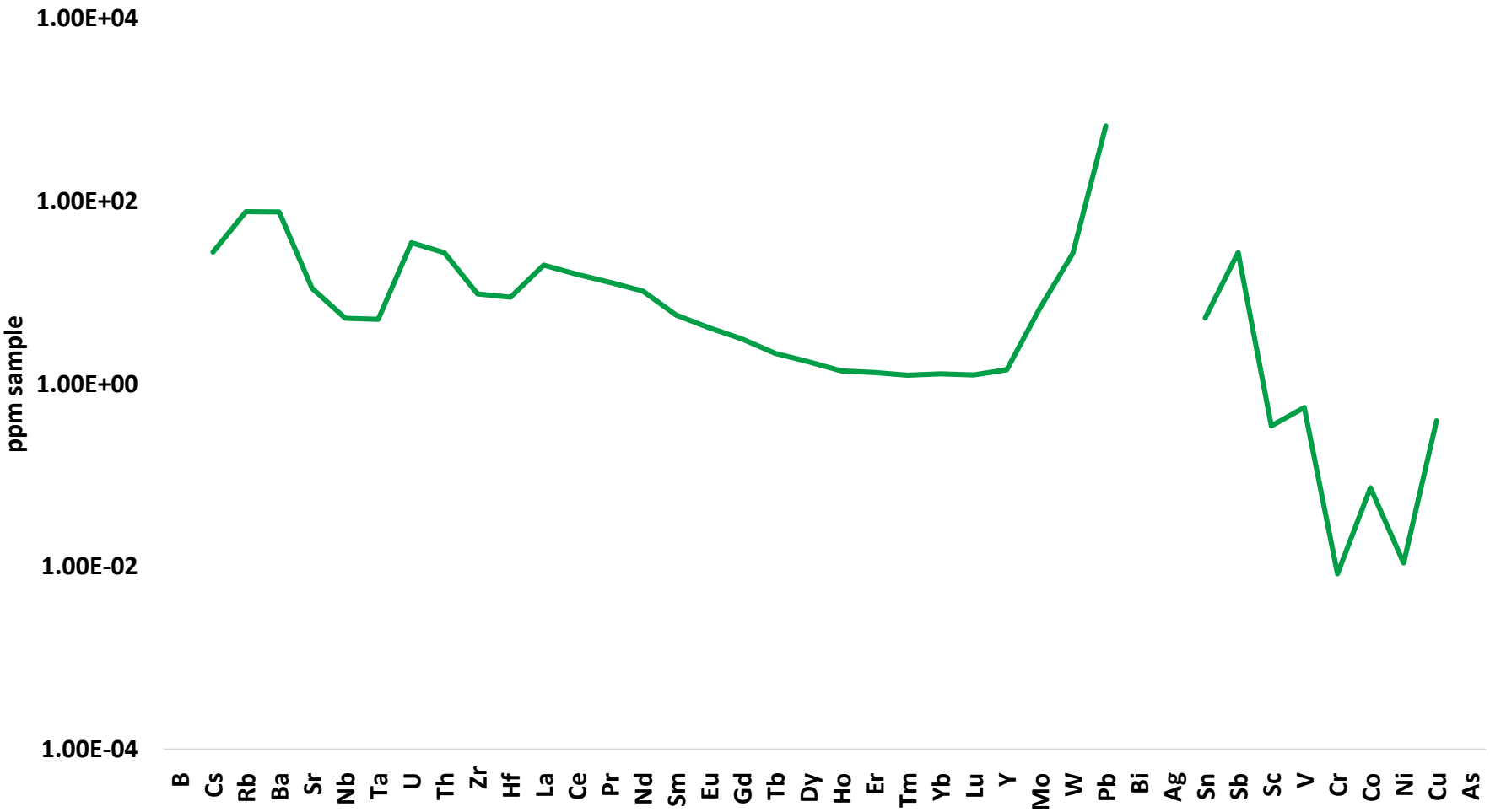

Figure 11. Trace element plot of the Pearl Lake porphyry. The green line displays the trace element concentrations obtained by bulk rock analysis. Melt inclusion analyses of the Pearl Lake porphyry were not obtained.

A strong correlation between the bulk and normalized melt inclusion analyses for the Paymaster and Crown localities shows an inversely sloping pattern, starting from left to right and finally the transition metals (Fig. 8 - 9). Upon comparison of the metal concentrations (Mo, W, Pb, Bi, Ag, Sn, Sb, Co, Ni, Cu, and As) in the bulk rock of the Paymaster, Crown and Pearl Lake localities, a very similar pattern can be seen going from left to right (Fig 10 – 13). Mo and W both show a strong positive trend in all 3 locations. The metals Sn, Sb, V, Co and Ni show a negative trend in the bulk rock analysis of the Crown and Pearl Lake porphyries, whereas the case is opposite for the Paymaster porphyry where the concentrations of those metals in the bulk rock are increasing. It should also be noted that the elements B, Ag and As are not accounted for in the bulk rock analyses for the Paymaster, Crown and Pearl Lake porphyries.

The melt inclusion analyses obtained from the quartz phenocrysts of the Paymaster and Crown porphyries depict enrichment of the incompatible elements B, Cs and Rb when compared to the bulk rock analyses of the two localities. The elements B, Cs and Rb are highly incompatible and are an indicator of the relative degree of evolution of the melt. These three elements tend to accumulate in the liquid and will not go into crystalizing phases. The Paymaster and Crown porphyries depict enrichment of the incompatible elements Ba and Rb.

When the bulk rock analysis of the Paymaster and Crown porphyries is compared to the melt inclusion analyses, it is seen that the LIL element Sr is enriched in the melts relative to the bulk rock. When compared to other elements in the figures it is seen that for the Krist fragmental unit as well as the Paymaster and Crown porphyries, Ba is enriched in the metals.

4.0 Discussion

4.1 major element and trace element discrimination and comparison of bulk rock and melt inclusion analyses

A Yb-Ta discrimination diagram (Fig. 12 A) was constructed that classifies different types of granitic magmas into four distinct categories: 1) volcanic arc granites (VAG), 2) syn-collision granites (synCOLG), 3) within plate granites (WPG), and 4) ocean ridge granites (ORG). These granitic setting define the global tectonic environments in which the parent magmas are generated. Melt inclusion analyses and bulk rock analyses of the Paymaster and Crown porphyries were plotted on the discrimination diagram along with the analyses of the Krist Fragmental, and a reliable result was observed to reside within (VAG) and (synCOLG). The cluster of points that was produced was under 10 on the Yb logarithmic scale and between 0.05 to just above 1 on the Ta logarithmic scale. Most of the points are in the VAG setting with some in the synCOLG setting. Both the Paymaster and Crown porphyry bulk analyses plot in the VAG setting. A TAS classification diagram (Figure 12 B) was constructed and classified the melt composition as dominantly dacitic. Trace element analyses (melt + bulk) for the Paymaster and Crown porphyries as well as the Krist fragmental unit confirm a geochemical link to adakite-like rocks (MacDonald 2010) (Fig. 8).

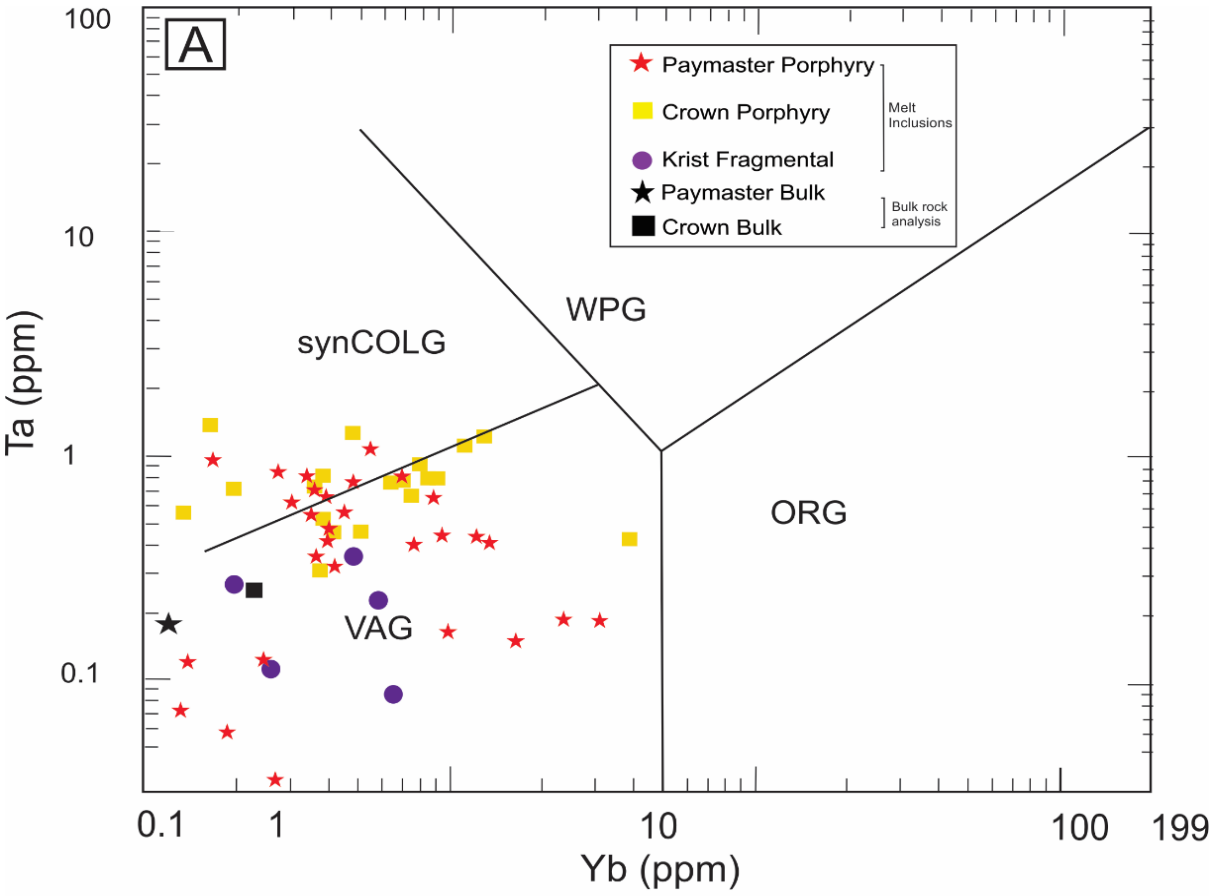
A
Paymaster Porphyry
Crown Porphyry
Krist Fragmental
Paymaster Bulk
Crown Bulk
Melt Inclusions
Bulk rock analysis
synCOLG
WPG
ORG
VAG
Ta (ppm)
Yb (ppm)
100
10
1
0.1
0.1
1
10
100
199

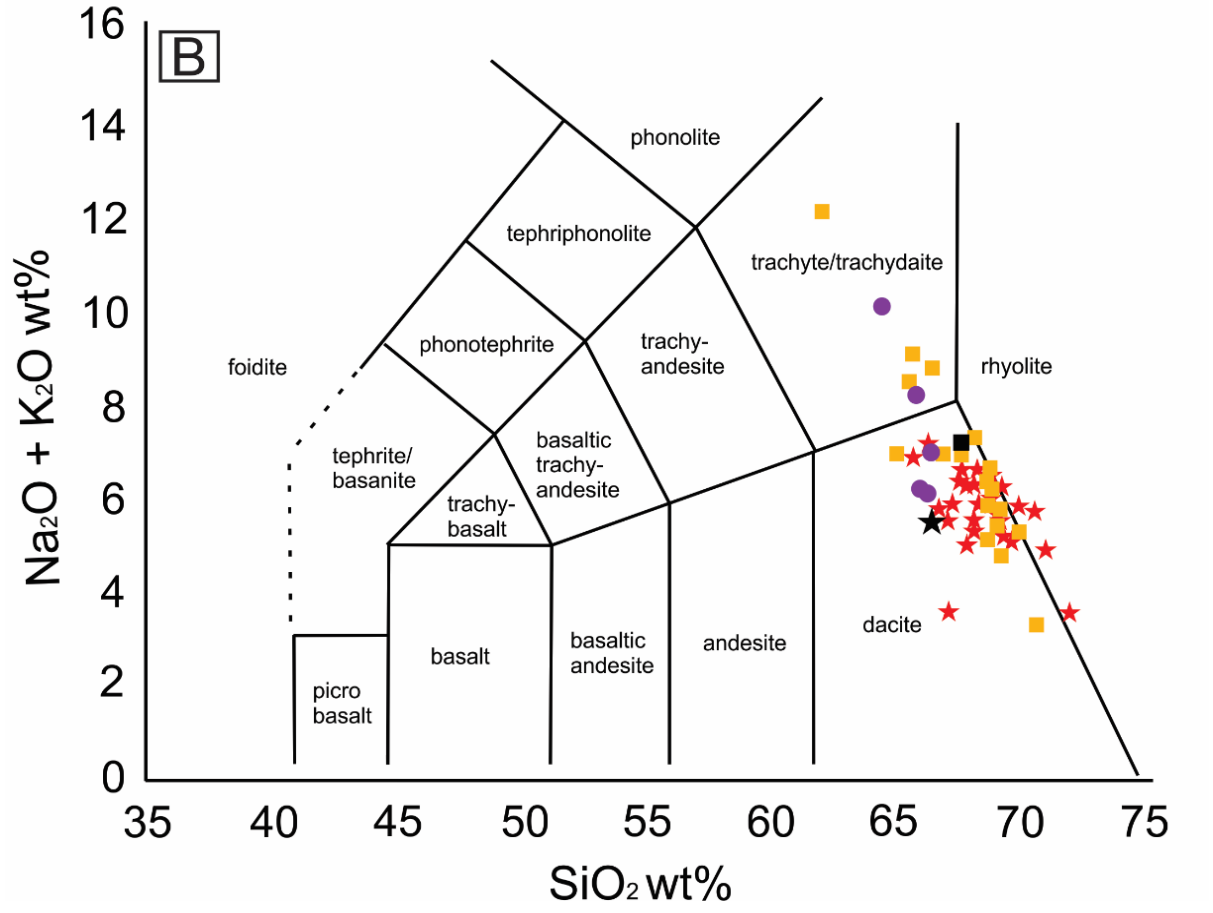
B
phonolite
tephriphonolite
trachyte/trachydaite
phonotephrite
trachy-andesite
foidite
rhyolite
tephrite/basanite
basaltic trachy-andesite
trachy-basalt
dacite
basalt
basaltic andesite
andesite
picro basalt
Na2O + K2O wt%
SiO2 wt%
16
14
12
10
8
6
4
2
0
35
40
45
50
55
60
65
70
75

Figure 12. (A) Yb and Ta raw data of LA-ICPMS analyses of the Paymaster and Crown Porphyries along with the analyses of the Krist fragmental plotted on the Ta-Yb discrimination diagram. The Bulk rock analyses of the Paymaster and Crown porphyries are also plotted on the discrimination diagram. This diagram separates different types of granitic settings into four distinct categories: 1) volcanic arc granites (VAG), 2) syn-collision granites (synCOLG), 3) within plate granites (WPG), and 4) ocean ridge granites (ORG). Most of the Paymaster and Crown melts are within the VAG setting. along with their bulk rock data. The Krist fragmental analyses also plot within the VAG. A few analyses of the Paymaster and Crown porphyries are in the synCOLG settting. This figure was modified from (Maanijou et al., 2012). (B) TAS classification diagram showing the region in which the melts of the Paymaster and Crown porphyries and the Krist fragmental unit fall. The bulk rock analyses of the three localities are also plotted.

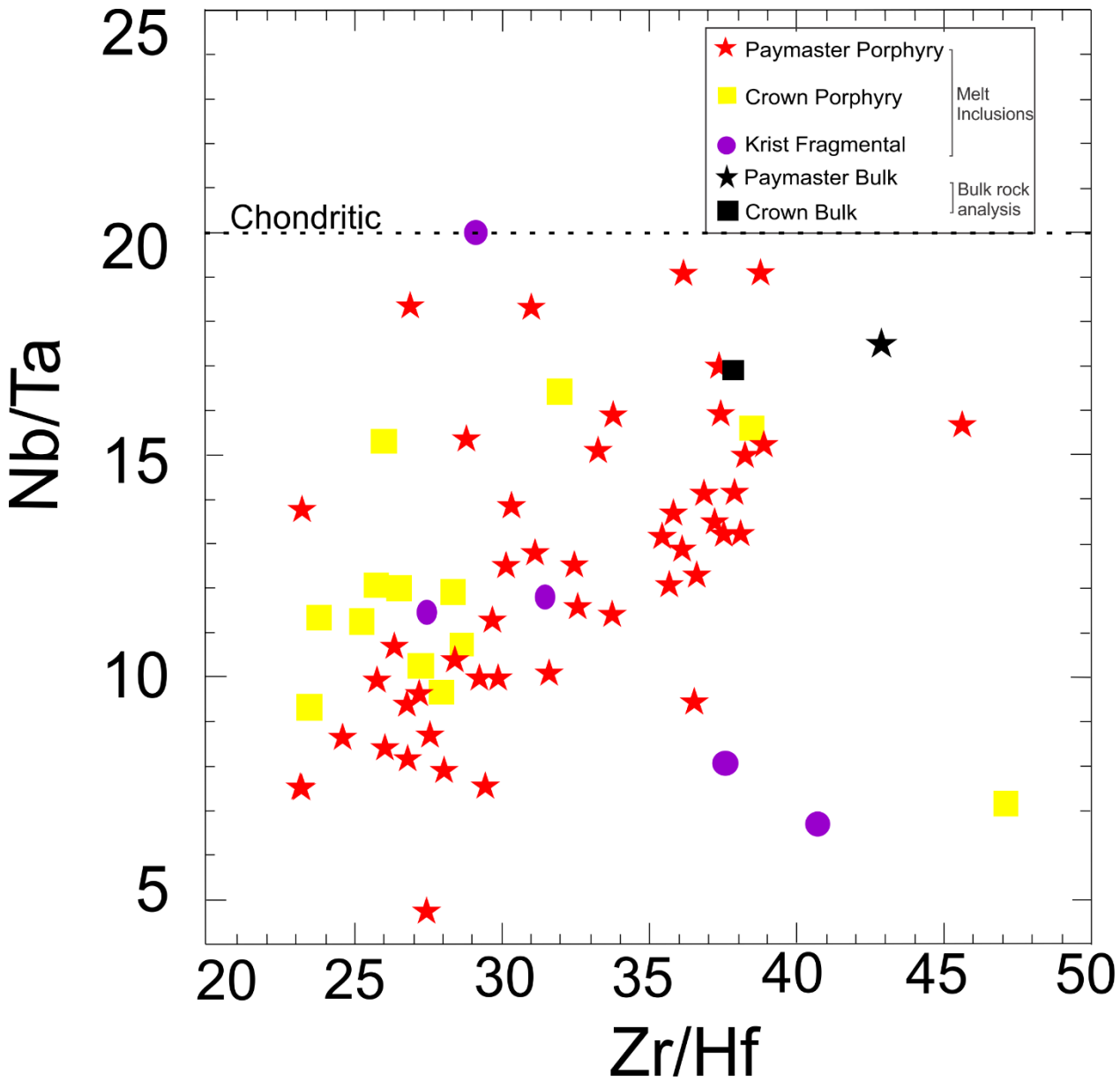

Figure 13. LA-ICPMS data from the melt inclusion analysis of the Paymaster and Crown porphyries along with their bulk rock analyses plotted and displayed on a Nb/Ta vs Zr/Hf ratio diagram.

The spider diagrams constructed for the normalized LA-ICP-MS melt inclusion analyses of the Paymaster and Crown porphyries along with the Krist Fragmental illustrate a negative anomaly for Nb (Fig. 10 – 12), indicating that there is Nb depletion in the melt, which shows that the source region was crystalizing rutile (Ti-rich) or one of its three polymorphs. The incompatible element Sr is enriched in the melt inclusions relative to the bulk rock of the Paymaster and Crown porphyries, but along with Eu it is depicting a negative anomaly, indicating that these elements have quite possibly substituted for the Ca and K in plagioclase and potassium feldspar (Fig. 10 - 12). The Rb-Ba-Sr ternary plot along with the melt inclusion data range illustrates that the system crystallized plagioclase at depth where the magma is residing (Fig. 19)

The metals Sn, Sb, V, Co and Ni are depleted in the bulk rocks of all three localities and even more so in the melt inclusion analyses of the Paymaster and Crown porphyries (Fig. 16 – 18). A strong depletion of these metals indicates that the source region contained some mafic rock bearing mafic minerals or was crystallizing minerals such as spinel, or chromite.

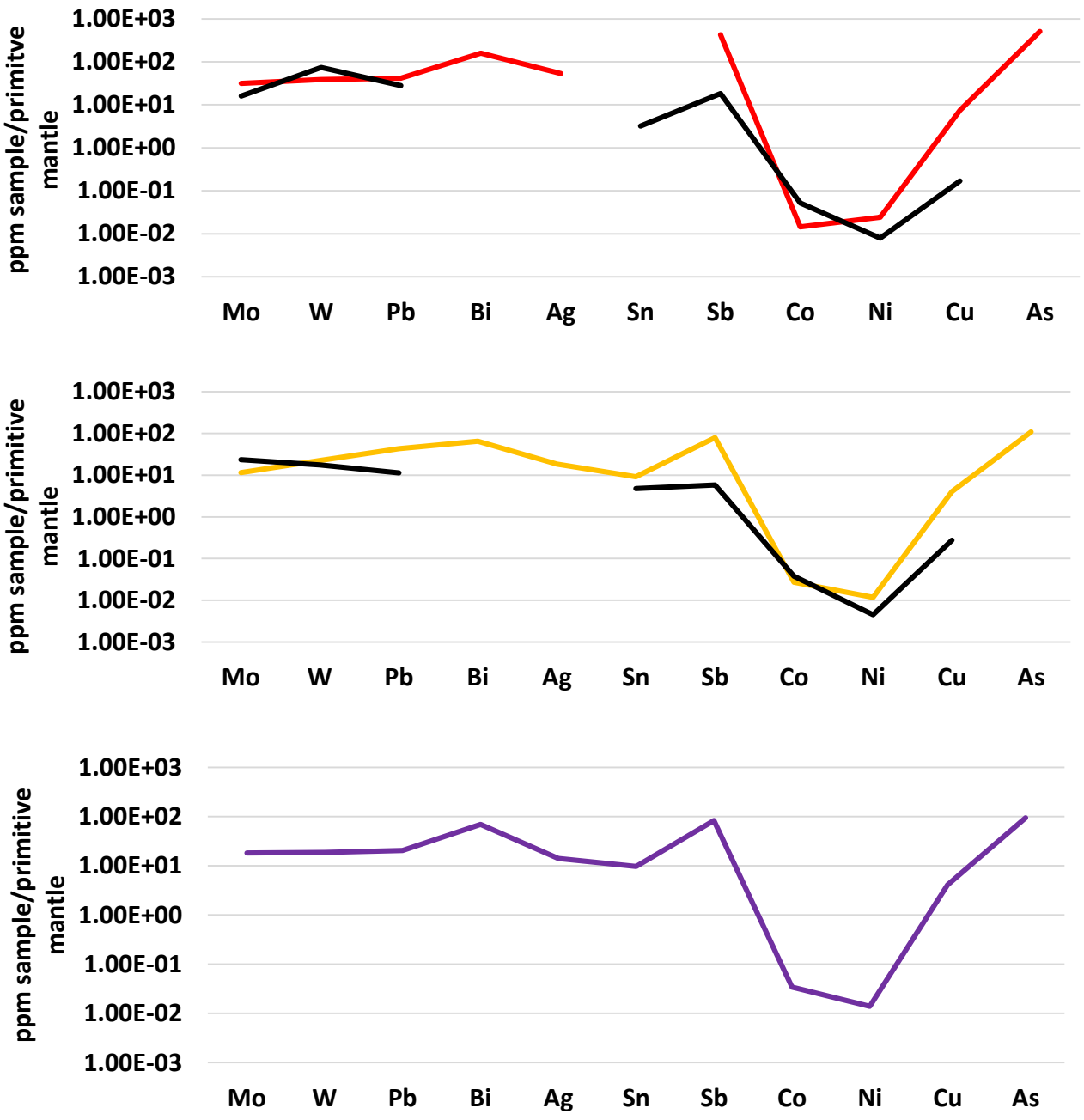

Figure 14. Comparison of metal concentrations of the melt inclusions analyses of Paymaster and Crown porphyries and the Krist fragmental unit relative to bulk rock analyses. The red, yellow and purple lines represent the Paymaster, Crown and Krist fragmental unit respectively. The black lines represent the bulk rock values for each locality. Bulk rock data for the Krist Fragmental was not obtained.

A strongly correlating downward trend from left to right is seen between the normalized trace element concentrations of the LA-ICP-MS analyses obtained for the Krist fragmental, Paymaster and Crown porphyries (Fig. 10 – 12). This trend is also true for the bulk rock data of the Paymaster, Crown and Pearl Lake porphyries and starts from the LILE, through the HFSE and all the way into the REEs (Fig. 10 – 11, 13). The elements Rb and Ba show enrichment in the melts, which indicates that the source region contains potassium-rich feldspar and micas. These two elements are both indicators for the same minerals and their enrichment in the melt inclusion data confirms that the source region contains K-feldspar and micas. The Paymaster and Crown porphyry REEs show a very gradual declining trend towards the HREEs (Fig. 11 – 12).

The spider diagrams of the Paymaster and Crown porphyries illustrate that Yb is depleted in some melts whereas it is enriched in the others relative to bulk rock. This suggests that the melt which has the highest concentration of Yb is the youngest, least evolved melt, whereas the melt which has the lowest concentration of Yb is the oldest, most evolved melt (Fig. 11 – 12). Yb is known to fractionate into garnets and the observation of a gradual decline towards the HREEs indicates possibly that there's trace amounts of garnets and zircons in the melt in the case where the concentration of Yb is low. The melt inclusion analyses depict a gradually declining trend of the LREEs, La, Ce, Pr, Nd, Pm, Sm and Eu. Some melt inclusion analyses are depleted in those metals relative to bulk rock while some are enriched. This indicates again that the melt inclusions with the highest concentration of the LREEs are part of the youngest, least evolved melt, whereas the melt inclusions with the least concentration of LREEs are part of the oldest, most evolved melt. (Fig. 11

– 13). The gradual decline indicates that trace concentrations of apatite and possibly monazite had begun crystallizing near the source region.

Similar to Nb and relative to other elements in the melt inclusion analyses such as B, Rb, Ba, Th and Bi, Ta is also slightly depleted. It is however enriched relative to bulk rock analyses of the Paymaster and Crown porphyries (Fig. 11 – 12). This quite possibly refers that the melt is crystalizing rutile (Ti-rich) or one of its three polymorphs, or other minerals such as ilmenite, titanite, columbite and tantalite.

When the information is compared to the petrography done on the Paymaster porphyry, the minerals observed confirm that the spider diagrams showcasing the elements are consistent with prominent minerals such as quartz, K-feldspar, plagioclase, minute amounts of pyrite and rutile as well as trace amounts of apatite, garnet, baddeleyite and zircon.

The melt inclusion data of the Krist Fragmental, Paymaster porphyry and Crown porphyry were shown to have considerably identical patterns (Fig. 11 – 13). Incompatible trace elements and elements such as Sr generally have high concentrations relative to bulk rock, with a few exceptions where the concentrations of these elements are low. The enrichment pattern informs us about the evolution of the melt. The melt inclusions with the highest concentrations of Sr are the youngest and least evolved, whereas a strong depletion indicates a more evolved melt. These patterns illustrate that plagioclase started to be removed from the source region between the time the youngest melt inclusion developed to the time the oldest melt inclusion developed.

The Rb-Ba-Sr ternary diagram (Fig. 18) confirms the trend of Sr that is being depicted by the melt inclusion data along with the bulk rock data of the Paymaster and Crown porphyries of the Timmins

District. This trend portrays that plagioclase fractionation is a major control on the evolution of the melt in the district. The depletion of Sr established by the LA-ICPMS melt inclusion data can be demonstrated by the removal of plagioclase crystals from the source region. This is feasible as the depletion of Sr is strongly correlated to the evolution of the melt.

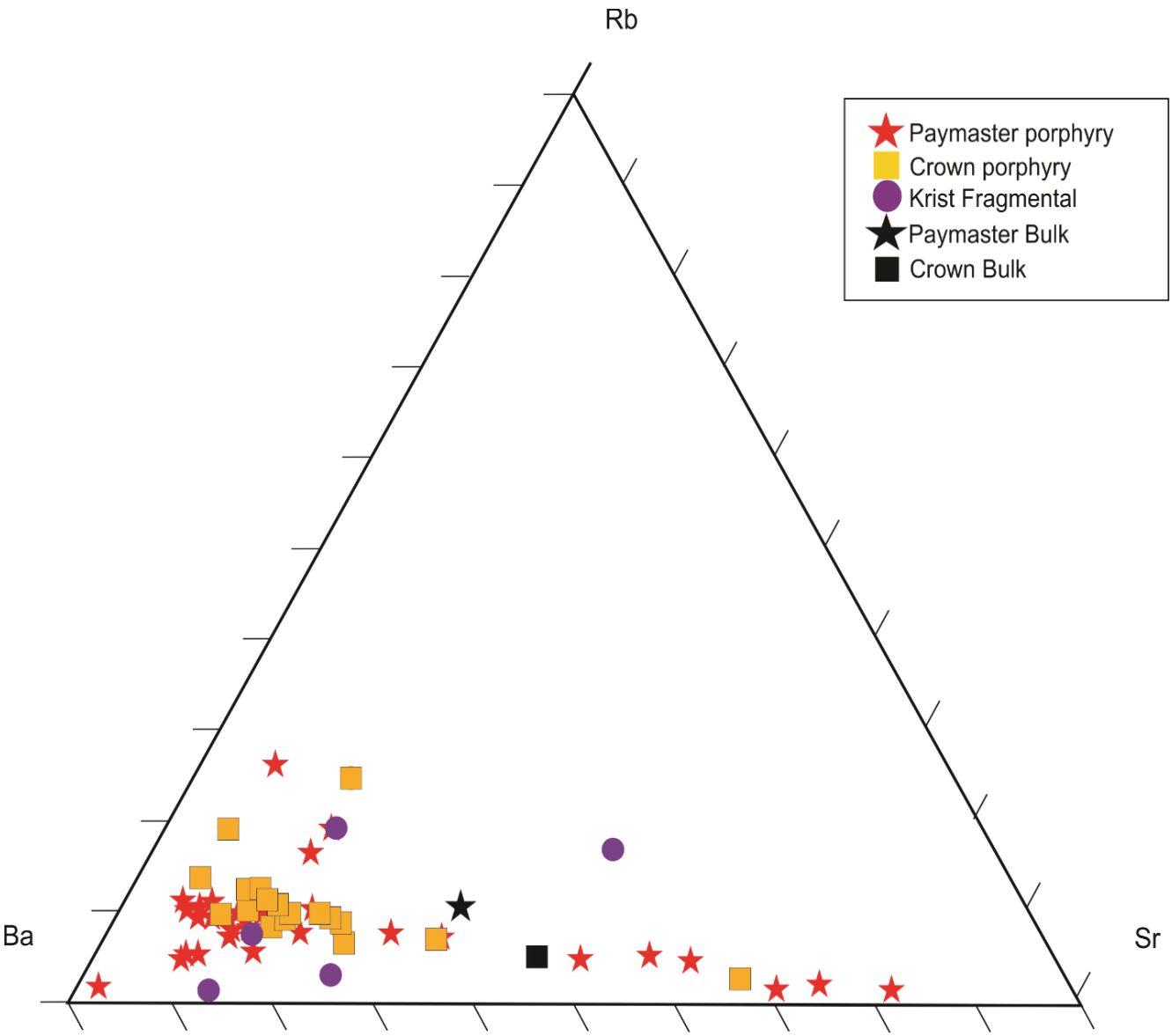

Figure 15. Rb-Sr-Ba ternary diagram depicting LA-ICPMS melt inclusion and bulk rock analyses of the Paymaster and Crown porphyries along with the Krist Fragmental of the Timmins District.

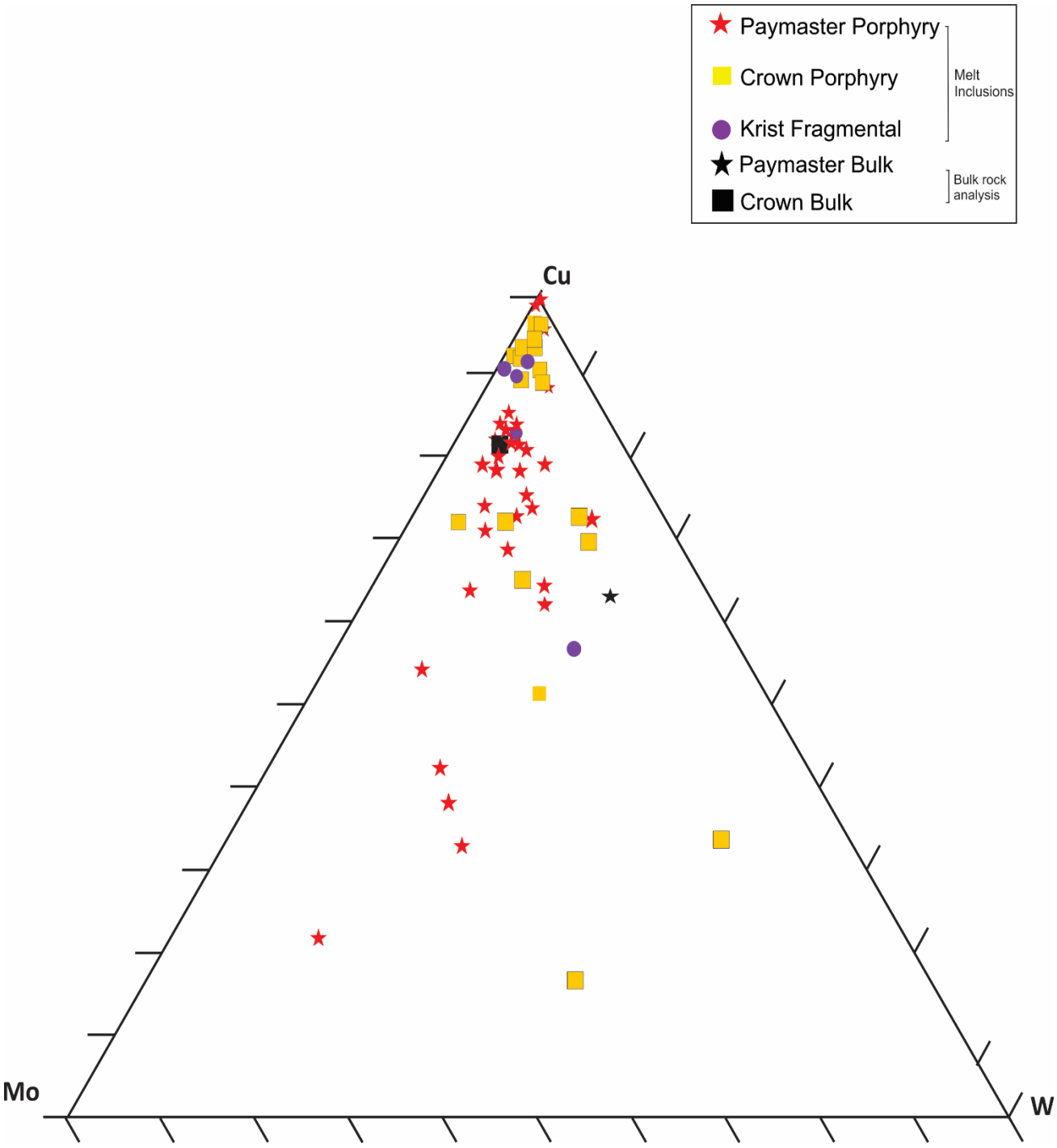

Figure 16. Cu-Mo-W ternary diagram depicting LA-ICPMS melt inclusion and bulk rock analyses of the Paymaster and Crown porphyries along with the Krist Fragmental of the Timmins District.

4.1.2 Correlation of metals

The metals Cu, Mo, Sn, Sb, Ag, W along with the elements As and B from the Paymaster and Crown porphyries as well as the Krist Fragmental were plotted against one another to see how they correlate to each other. B was found to have good correlations with As, Cu, Mo, Sb and the ratio of Cu/Mo. The trends shown by the plots illustrate that as the concentration of B in the melt increased, so did the concentration of As, Cu, Mo and Sb (Fig. 20).

The Cu/Mo ratio in the melt also shows a positively increasing trend with B, however, the trend with W seems to be decreasing. This means that as the W concentration in the melt for the three localities was increasing as the ratio of Cu/Mo was decreasing. The HFSE Nb and Ta display a strong positive correlation (Fig. 21) in all three localities. An increase in the Nb concentration lead to an increase in the concentration of Ta synonymously (Fig. 22). This can conclude that the melts with low concentrations of Nb and Ta correspond to the time when minerals such as rutile, ilmenite, titanite, columbite and tantalite started to crystallize. A similar trend can be seen for the Mo and W (Fig. 22), where it is clear that there is a directly proportional relationship between the increase in concentrations of Mo and W.

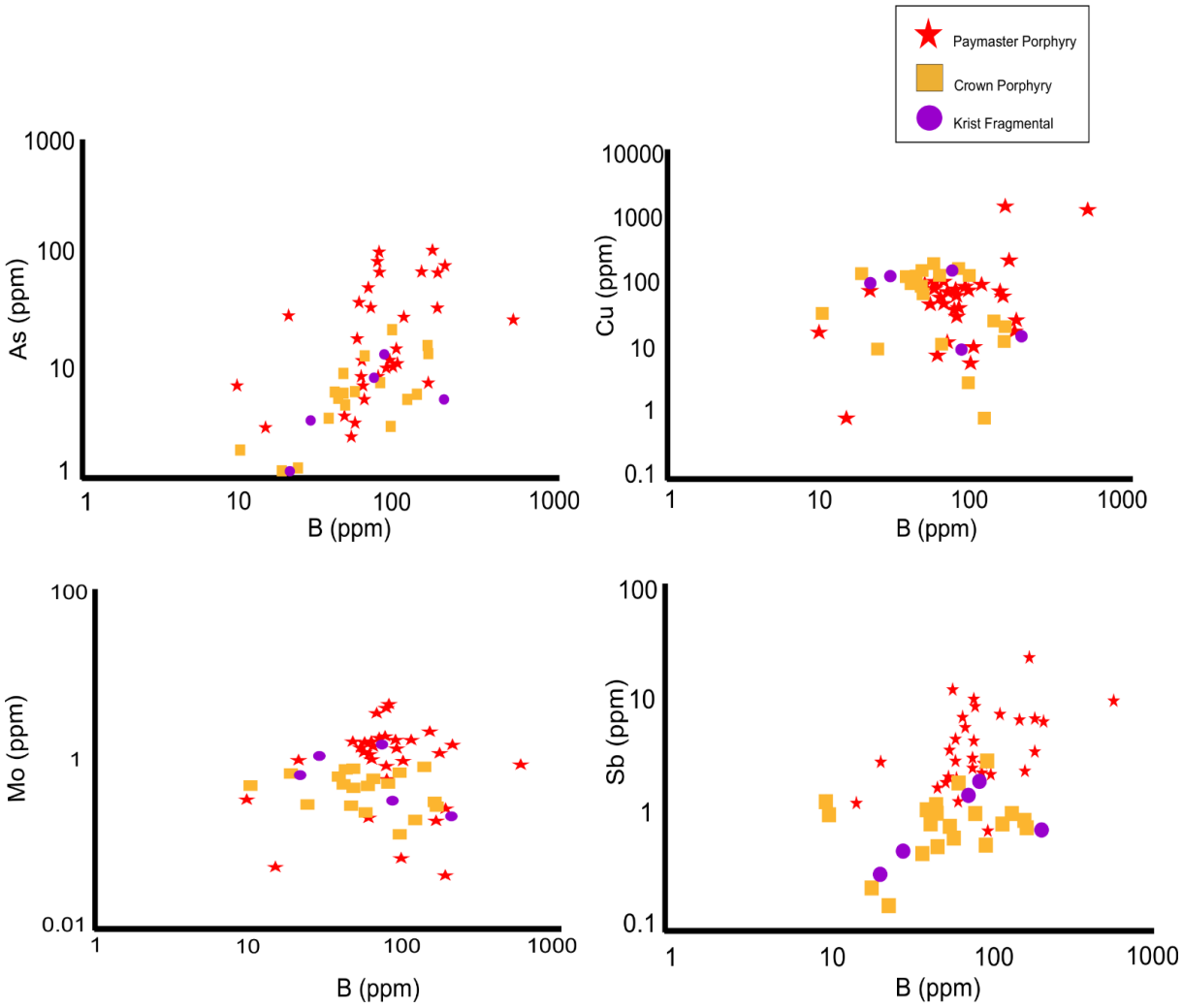

Figure 17. Multi figure panel illustrating the relationship of metals in the Paymaster and Crown porphyries and the Krist felsic volcanic rocks of Timmins

.

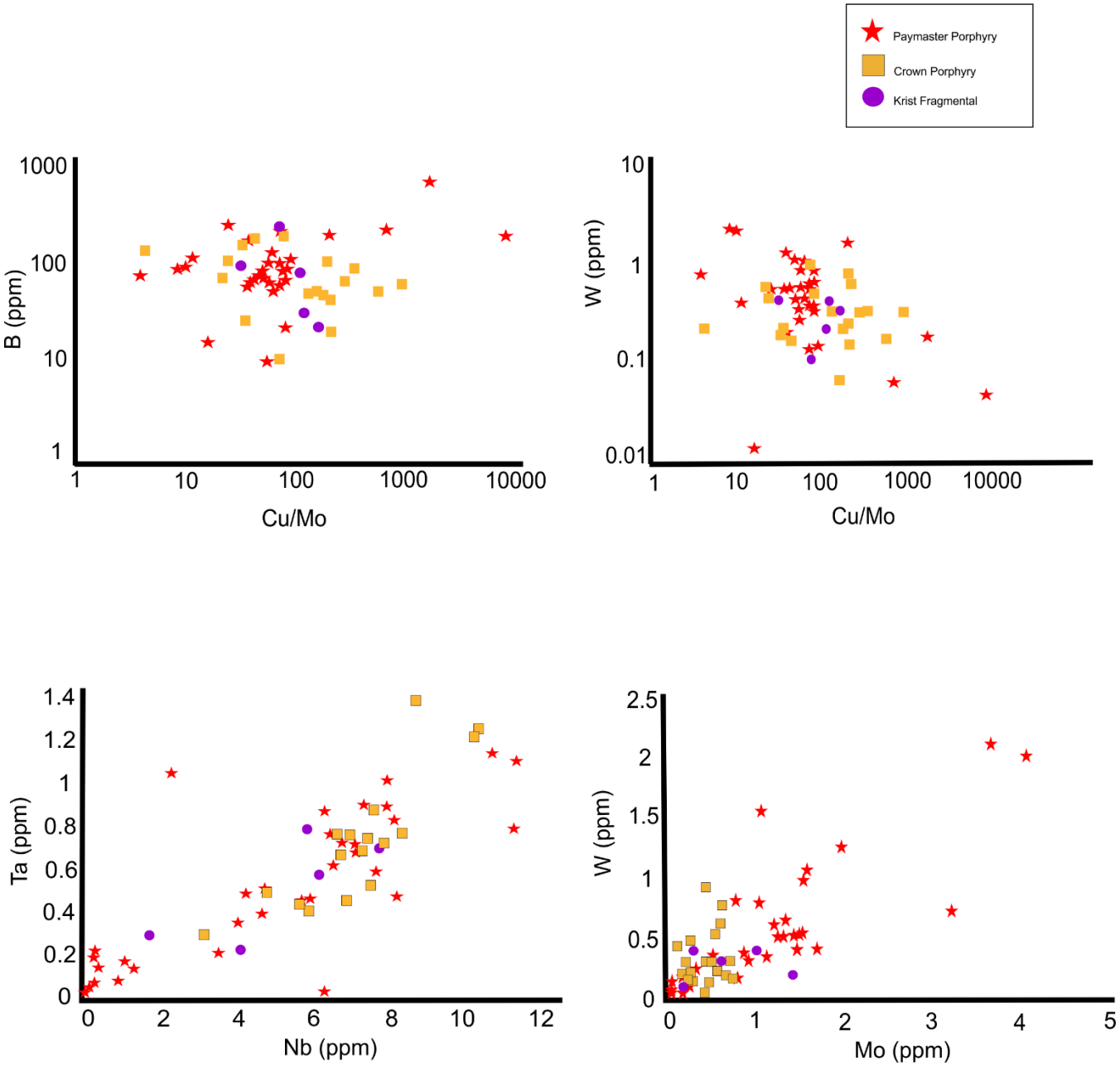

Figure 18. Multi figure panel illustrating the relationship of metals in the Paymaster and Crown porphyries and the Krist fragmental of Timmins.

If we observe the spider diagrams for the Paymaster and Crown porphyries (Fig. 11 – 12), it is clear that the Mo and Cu content is higher in the melt than it is in the actual bulk rock. (Audétat et al. 2008)described various factors as to why this may be so in a magmatic-hydrothermal system. Selective metal precipitation has a large influence on the ore metal ratios, explaining how a pure Mo deposit could form at Questa and an essentially pure Sn deposit in the Mole Granite, Australia, despite Cu, Pb and Zn in the input fluids up to one order of magnitude higher than those of Mo and Sn, respectively ((Audetat et al. 1998, Audétat et al. 2008, Klemm et al. 2008); Tables 2, 3, App.). However, selective metal precipitation may not have been the only factor in control of the ore metal ratios as for some elements there is a distinct correlation between ore type and the composition of the magmatic parent fluid (Audétat et al. 2008, Table 2, pg 897.)

Fluid immiscibility and related vapor-brine partitioning of ore metals may affect the mineralization process in several ways, including: (1) ore precipitation as a direct consequence of fluid boiling and associated loss of H_2S (among other things); (2) physical separation of chemically contrasting fluids, leading to system-scale metal zonation; and (3) accumulation of chlorine-complexed metals in residual brine (Audétat et al. 2008). Drummond and Ohmoto (1985) showed that the first process was an efficient mechanism for Au precipitation in shallow epithermal deposits as well as deeper orogenic deposits where vapor exsolves from liquid-dominated fluids. Contrasting metal partitioning between vapor and brine phases as a result of their immiscibility leads to chlorine-complexed elements fractionating into the brine, and S, Cu, As, Au, B (± Li, Sb) fractionating into the vapor phase (Heinrich et al., 1999; Williams-jones and Heinrich, 2005).

Condensation of brine from a low-density parental fluid and its accumulation at depth could be an efficient process to concentrate chlorine-complexed metals in a small rock volume, leading to ore formation at deeper levels of magmatic-hydrothermal systems (Audétat et al., 2008). High solubilities in the brine phase as opposed to the vapor phase of the metals Sn, W, Mo, Ree and the tendency of brines to occupy much smaller volumes than the same mass of a vapor phase increases the likelihood of metal precipitation in a small rock volume. This also leads to several lines of evidence suggesting that brines indeed played a critical role in the formation of many types of magmatic-hydrothermal deposits despite representing only a small fraction of the total fluid exsolved from the associated intrusion (Audétat et al., 2008).

The correlation between fluid composition and the type of mineralization for Mo, Sn, W and Ce is higher in the brines than in the low salinity fluids and secondly, intrusion scale mapping conducted by John (1989) and Ratajeski and Campbell (1994) informs of a clear correlation between the abundancy of brine inclusions and the occurrence of Cu, Pb, Zn, Ag and REE mineralization (Audétat et al., 2008). The correlation noted by John (1989) described that most hydrothermal mineralization is associated spatially with sections of the intrusion where high-salinity fluids are present. Ratajeski and Campbell (1964) found that vapor-rich inclusions are abundant in quartz phenocrysts but scarce in vein quartz, leading to the conclusion that it is difficult to envisage veins in the Capitan pluton forming by anything other than a brine-dominated fluid.

Fluid evolution trends recorded in individual quartz crystals from vein deposits within the Mole Granite display more evidence as to brines playing a major role in the formation of some magmatic-

hydrothermal deposits. Sn, W and Bi ore formation in the Mole Granite intrusion were caused by mixing of meteoric fluid and magma-derived fluids and are recorded in the brine by Sn, W and Bi concentrations that decrease sharply than those of nonprecipitating elements such as Na, K, Cs and Pb (Sun and Eadington, 1987, Audétat et al., 1998, 2000b). Synonymously, the concentrations of the vapor-fractionating elements such as Cu, B and Li in the brine increased relative to Na, K, Cs and Pb. This observation can not hold true if vapor is the dominant phase in the veins because the concentrations of C, B and Li in this case should have decreased in both the vapor and brine phase (in the vapor due to addition of meteoric water and in the brine because the concentrations can only mimic the compositional evolution of the vapor if the brine/vapor mass ratio is small) (Audétat et al., 2008).

This trend suggests that the brine phase dominated the ore-forming fluid and that the meteoric water was enriched in Cu, B and Li due to condensation of the vapor phase into it. The fluid evolution in the veins of the Mole Granite is described by Audetat et al., (2008) in four steps; (1) exsolution of a vapor rich, single-phase fluid from the crystallizing magma; (2) condensation of brine form this fluid; (3) accumulation of brine in the lower portions of the vein system while vapor escapes upward and is condensed by meteoric water; (4) incursion of the meteoric water into the pluton interior, causing ore precipitation upon mixing with brine (Audétat et al., 2008). This model suggests that sequestering of Mo by brine and the concomitant escape of Cu-rich vapor was one of the reasons why no Cu is present in the Questa deposit despite a Cu/Mo ratio of about 70 by weight in the single-phase bulk fluid (Klemm et al., 2008). To further support this, porphyry Cu deposits have an abundance of brine inclusions similar to that of vapor inclusions, and brine inclusions seem

to be particularly abundant in the area of mineralization (Roedder, 1971; Moore and Nash, 1974; Eastoe, 1982; Bodnar, 1995; Roedder and Bodnar, 1997). Observations made by Audétat et al., 2008 concluding that the sequestering of Mo by brine and the escape of a Cu-rich vapor can possibly explain why the Cu is depleted in the bulk rock analyses of the Paymaster and Crown porphyries.

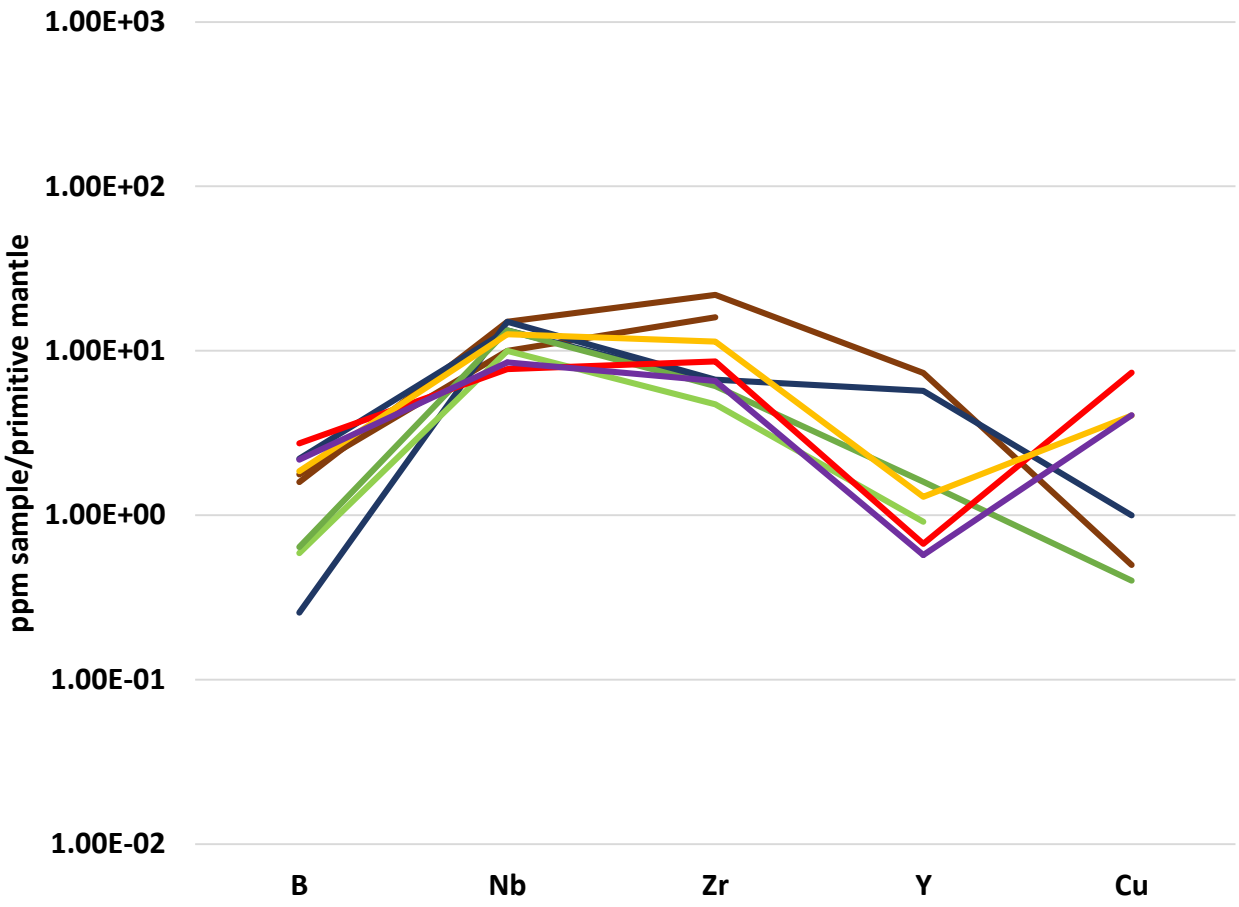

Figure 19. comparison of mineralized modern porphyry systems (Cretaceous) and ancient porphyry systems (Archean). The red, yellow and purple lines represent the average trace element values of the Paymaster and Crown porphyries and the Krist Fragmental in Timmins. The brown, dark blue and green lines represent the Hornblende-Diorite, Quartz-Monzodiorite and Rhyodacite in the porphyry-Cu mineralized Santa Rita deposit, New Mexico (USA)

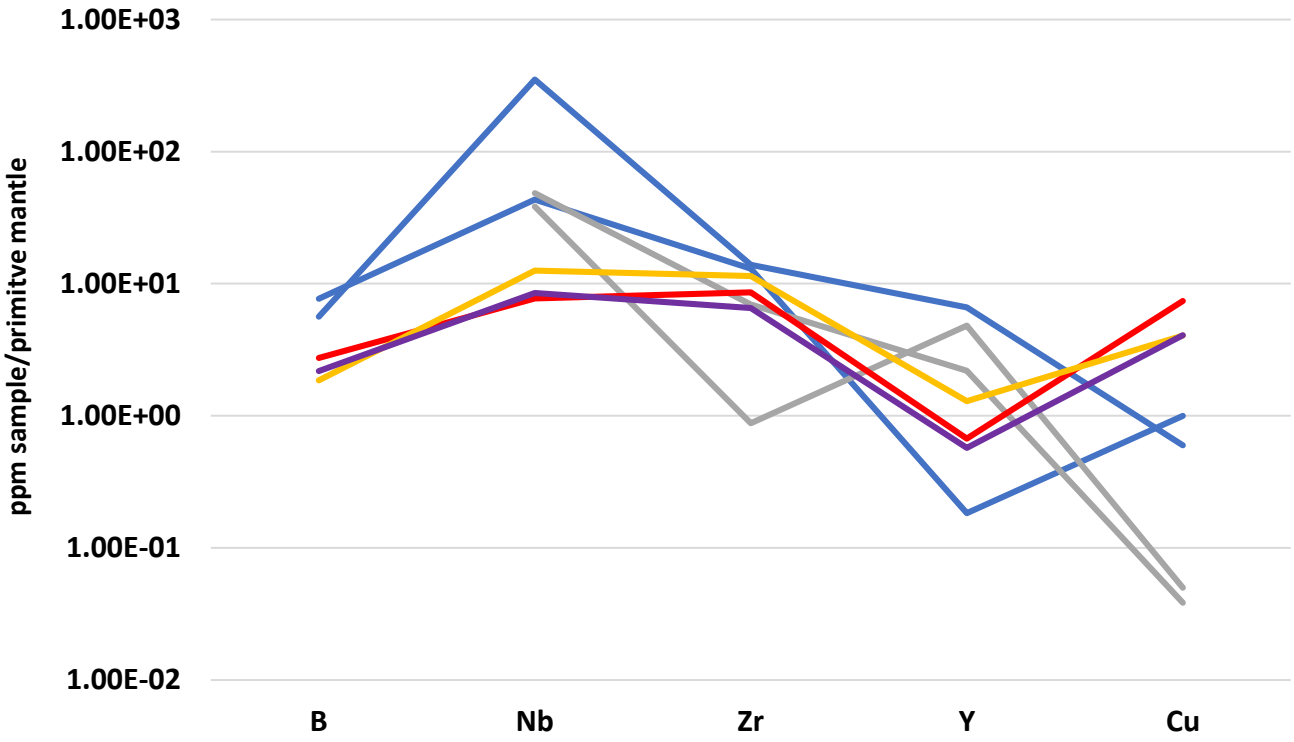

Figure 20. comparison of modern (Paleogene) barren granites to ancient (Archean) porphyry systems. The red, yellow and purple lines represent the average trace element values of the Paymaster and Crown porphyries and the Krist Fragmental in Timmins. The light blue and grey lines represent the Rito del Medio and Canada Pinabete plutons in northern New Mexico (USA).

4.2 *Evolution of magma and Cu degassing in the Archean*

A Sr/Y vs Y and $(La/Yb)_N$ vs $(Yb)_N$ plot was constructed to illustrate that the melt inclusions from the Paymaster and Crown porphyries along with the Krist framgnetal all fall in the adakite area as indicated. (Fig. 21) The trend shown in the Sr/Y vs Y plot shows that the decrease in the concentration of Y in the melt falls in conjunction with the trends known to be displayed by the formation of adakites, and it is interesting to recognize this trend in melt inclusions that are 2.7 Ga old.

The trend that is shown by the decrease in Y is a result of a cooling, evolving melt that has some samples of it being trapped in crystal, confirming that the minerals that are crystalizing are trapping Y. An adakite is formed by partial melting of not only the mantle as in a normal subduction zone setting, but also the oceanic crust, which contains tholeiitic magma and is quite rich in Al. Excess Al in an adikitic magma results in the crystallization of the minerals amphibole and clinopyroxene, with amphibole being a key mineral in adikites and strongly compatible with HREEs. This compatibility explains the decrease in the Y concentration in the melts as the Y would have been partitioned into the amphiboles, and also possibly points to the crystallization of amphibole and clinopyroxene in magma chambers 2.7 Ga below the now Timmins district. This trend is exhibited by all three localities involved in this study and is an evidence of large, evolutionary compositional ranges in chemistry in its source region before emplacement.

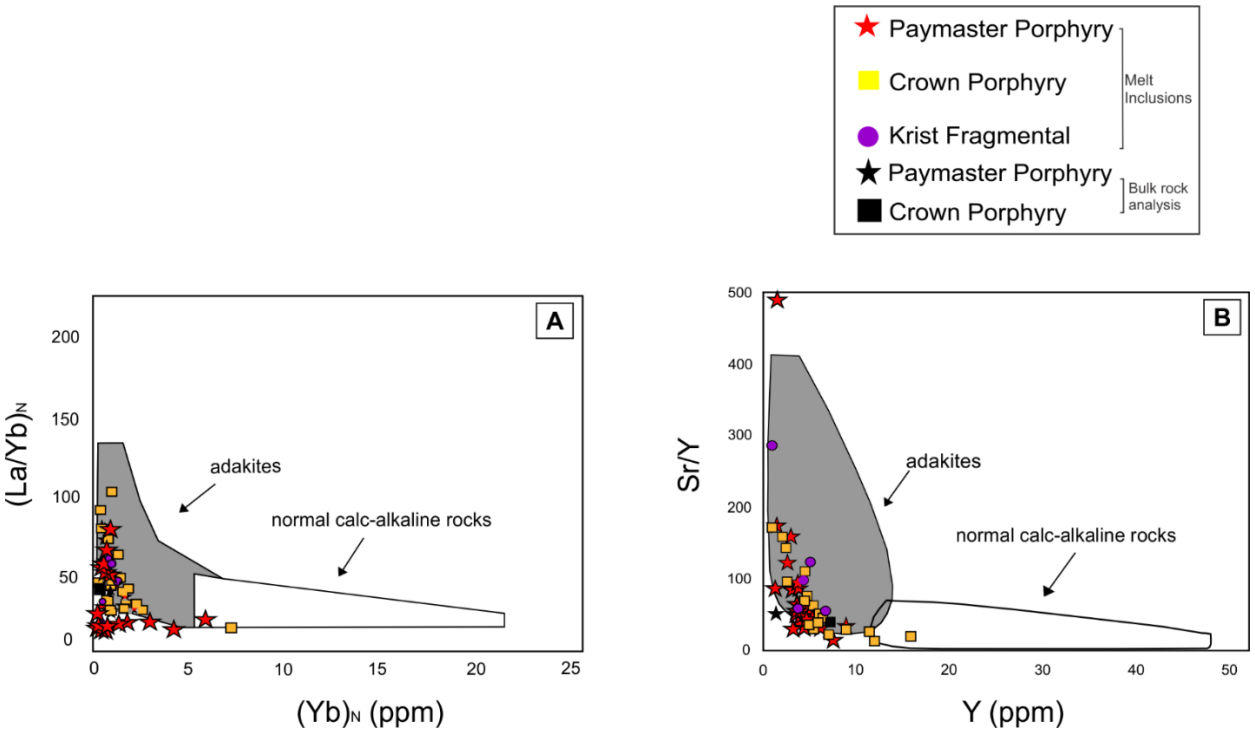

Figure 21. Discrimination plots for the Paymaster and Crown porphyries and the Krist fragmental unit of Timmins. (A) $(La/Yb)_N$ versus $(Yb)_N$ normalized to primitive mantle plot illustrating the relative positioning of the melts from the three localities; (B) Sr/Y versus Y diagram illustrating the relative positioning of the melts from the three localities. (Modified from (Moyen, 2004)

As discussed above, the high Sr and low Y values indicate the crystallization and accumulation of amphibole and pyroxene at depth. A similar trend is also shown by Nb where a depletion in the concentrations of Nb is complimented by an increase in the concentration of Ta. This represents the evolution of the melt and inclusions that have undergone fractionation. A similar trend is shown yet again by Sr/Y vs Cu where there's a shift to lower Cu values as we start increasing the Sr/Y ratio. The important pattern to notice is that this is opposite of what we would expect along the adikite trend, as magmas that are adikitic have higher Cu concentrations and produce porphyry deposits as a result. But it is evident by looking at (Fig) that the Cu concentration is decreasing as a result of fractionation. This could be explained by two possibilities.

The first possibility could be that the Cu content in the melt is decreasing due to the fact that it is going in mineral phases that are crystallizing. A second possibility could be that the crystals that are growing have reached a point where the rate at which they extract water out of the magma is increased by the water content in residual liquid. this would mean that the residual magma is at a point of, or is approaching, fluid saturation. Once that saturation point is reached the fluid will leave the magma, taking the Cu along with it. This decrease in Cu content could possibly be evidence of Cu degassing in an Archean porphyry system (Fig.22). The trend illustrated by the Nb/Ta ratio supports this claim

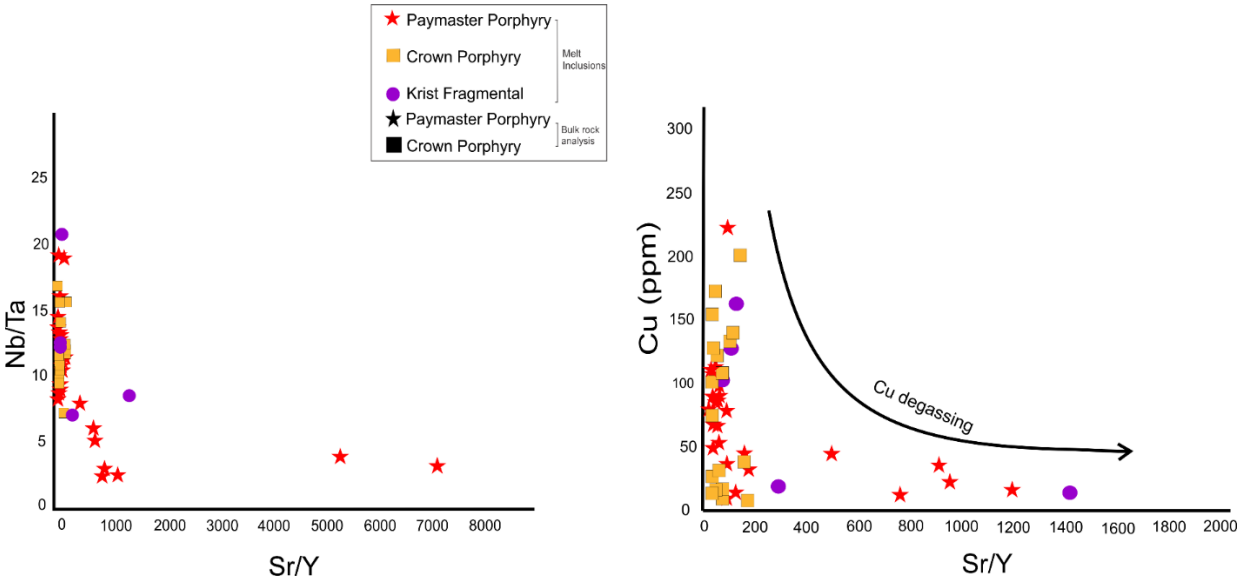

Figure 22. (A) Sr/Y versus Nb/Ta plot showing the inversely proportional relationship between Sr and Nb (B) Sr/Y versus Cu plot illustrating Cu loss to magmatic fluid degassing.

5.0 Conclusions

The data obtained from the melt inclusion analyses have confirmed that quantification of metal content of Archean age rocks is possible. Discrimination plots and spider diagrams have allowed us to construct and display the trends carried out by trace elements present in the magma chamber in the Archean. SEM data has shown that Cu and Au coprecipitated in the porphyries and this implies that Cu and Au are related, therefore any processes that affected Cu might have also affected Au.

The melts from the Paymaster and Crown porphyry along with the Krist fragmental unit are all falling in the adakitic field. The adakitic trend that is shown by these melts and cannot be portrayed by bulk rock analyses, which leads to the necessity of melt inclusion analyses to provide evidence of fractionation of magmas at depth following the adakitic evolutionary trend.

The Paymaster and Crown porphyry melt inclusion analyses along with those from the Krist fragmental unit demonstrate that melts in these systems were sourced from the same parental magma. There is a ~10 Ma time gap between the porphyries and the Krist fragmental unit. This, combined with the melt inclusion data indicates that the parental melt reservoir did not change much over the ~10 Ma magmatic window with a large metal rich reservoir at depth that was fractionating.

Tools such as the $(La/Yb)_N$ vs $(Yb)_N$, Sr/Y vs Y vs and Nb/Ta vs Zr/Hf plots combined with plots of Sr/Y vs Cu have illustrated a relationship between the fractionation of incompatible trace elements and the magmatic-hydrothermal behaviour of metals. In this example the Nb, Ta and Cu concentrations seem to be following trends that are not explained by the crystallization of minerals

in a magma chamber at depth, but possibly inform us about metal loss due to degassing in Archean porphyry systems.

Table X - LA-ICPMS analyses of single melt inclusions in porphyry intrusions and porphyry fragments within volcanics

Ablation File	Host	Assemb.	SiO2	TiO2	Al2O3	Fe2O3	FeO	MnO	MgO	CaO	Na2O	K2O	P2O5	B	Cs	Rb	Ba	Sr	Nb	Ta	U	Th	Zr	Hf	La	Ce
2017_01_12a08.csv	Paymaster	1	67.1	0.418	19.6	0	0.913	0.007	0.4488	0.528	1.36	5.09	0.071	177	20.4	175	3111	311	7.28	0.837	2.59	5.43	121	4.77	5.13	8.52
2017_01_12a09.csv	Paymaster	1	68.3	0.311	19.6	0	0.908	0.002	0.234	0.319	0.972	4.821	0.073	104	11.4	153	2635	268	7.06	0.658	1.59	7.68	83	3.47	7.57	17.6
2017_01_12a10.csv	Paymaster	1	66.6	0.194	19.6	0	1.17	0.0305	0.7422	1.69	1.69	3.73	<0.078	216	26.3	155	2412	288	6.72	0.671	2.91	4.22	108	3.95	15.97	30.2
2017_01_12a11.csv	Paymaster	1	68.5	0.319	19.6	0	0.708	0.006	0.4939	<0.20615	1.11	4.45	<0.220	79.6	5.06	106	1476	289	0.362	0.196	0.19	0.433	8.29	0.653	0.48	0.232
2017_01_12a13.csv	Paymaster	2	67.8	0.18	19.6	0	1.135	0.017	0.257	0.714	0.838	4.95	0.027	78.2	5.57	130	1220	216	4.72	0.475	2.48	7.57	108	4.62	22.2	42.9
2017_01_12a14.csv	Paymaster	2	68.3	0.147	19.6	0	0.763	0.004	0.2103	0.161	0.686	5.64	<0.037	92.9	6.73	152	1297	127	6.4	0.708	2.52	5.23	64.2	3.52	18.2	35.3
2017_01_12a15.csv	Paymaster	3	67.5	0.072	19.6	0	1.2	0.011	0.8603	0.08	0.791	5.33	<0.003	193	4.72	187	767	178	1.36	0.124	0.341	1.01	43.4	3.03	1.75	0.795
2017_01_12a16.csv	Paymaster	3	69.1	0.171	19.6	0	0.929	0.009	0.7167	0.075	1.68	3.29	<0.015	193	5.94	80	667	377	2.32	0.968	0.183	0.98	26.5	2.6	0.046	0.198
2017_01_12a19.csv	Paymaster	4	67.3	0.238	19.6	0	1.1	0.024	0.2712	0.773	0.732	5.40	0.025	63.3	6.7	146	1270	202	7.88	0.822	3.16	8.73	113.9	4.55	25.6	50.7
2017_01_12a18.csv	Paymaster	6	70.4	0.098	19.6	0	0.052	0.0078	0.1712	0.42	3.51	1.27	<0.048	82.1	2.93	45	375	625	1.16	0.156	1.55	3.18	35.2	1.72	9.61	24.1
2017_01_12a23.csv	Paymaster	4	65.8	1.003	19.6	0	<0.034	0.006	0.109	2.97	5.14	1.89	<0.226	593	15.8	34	267	374	0.438	0.126	0.087	0.05	1.21	0.297	0.11	0.397
2017_01_12a23.csv	Paymaster	6	69.9	0.058	19.6	0	<0.024	<0.002	0.0378	0.761	4.43	1.16	<0.188	68.7	2.41	23	281	855	0.313	0.171	0.354	0.182	1.84	1.2	5.88	7.51
2017_01_12a29.csv	Paymaster	1	68.2	0.139	19.6	0	1.03	0.01	0.24	0.25	0.76	5.28	0.03	57.7	6.71	152	1163	121	5.91	0.426	2.18	6.73	82.8	3.06	24.6	48.1
2017_01_12a30.csv	Paymaster	1	66.1	0.148	19.6	0	1.28	0.03	0.76	1.90	0.76	4.90	0.02	21.1	3.17	132	934	251	4.03	0.321	1.36	4.07	73.6	2.58	17.9	33.7
2017_01_12a31.csv	Paymaster	2	68.7	0.149	19.6	0	0.628	0.005	0.199	<0.218	0.734	5.330	<0.211	153	5.9	144	1090	81.3	6.28	<0.405	1.68	1.49	63.3	2.35	3.41	6.41
2017_01_12a32.csv	Paymaster	2	68.2	0.152	19.6	0	0.833	0.012	0.177	0.746	0.522	5.240	<0.050	61.8	6.91	154	1192	115	7.6	0.547	2.59	8.16	58.01	2.83	25.3	50.2
2017_01_12a33.csv	Paymaster	3	68.2	0.080	19.6	0	0.965	0.007	0.695	0.032	0.521	5.370	0.002	98.4	6.25	230	585	65.9	0.95	0.074	0.386	0.869	25.5	1.31	0.491	1.01
2017_01_12a34.csv	Paymaster	3	67.2	0.145	19.6	0	1.12	0.03	0.25	1.11	1.51	4.71	0.02	48.3	4.11	122	957	181	4.65	0.361	1.85	5.41	92.07	3.11	20.2	38.9
2017_01_12a42.csv	Paymaster	x	65.2	0.126	19.6	0	1.820	0.023	1.105	0.97	4.27	2.44	0.018	64.6	3.967	252	837	211	6.49	0.572	1.92	22.3	80.7	3.09	16.7	31.9
2017_01_12a43.csv	Paymaster	x	65.3	0.009	19.6	0	0.289	0.002	0.136	3.36	5.83	0.97	<0.032	<9.77	1.27	45.5	445	464	0.338	<0.060	0.538	11.1	11.2	0.683	9.57	16.2
2017_01_12a44.csv	Paymaster	x	67.3	0.108	19.6	0	0.935	0.031	0.190	2.23	1.29	3.80	0.024	62.1	5.47	120	1143	178	8.08	0.77	2.48	6.95	95.4	3.598	21.7	41.6
2017_01_12a43.csv	Paymaster	x2	68.7	0.145	19.6	0	0.993	0.017	0.217	0.923	0.616	4.29	<0.027	53.5	5.42	106	1013	264	5.69	0.42	3.73	9.3	857	20.5	24.2	46.6
2017_01_12a47.csv	Paymaster	1	67.8	0.186	19.6	0	1.049	0.006	0.269	0.137	0.916	5.57	0.037	115	8.79	169	1444	160	7.91	0.941	3.12	11.9	49.01	2.06	40.5	79.6
2017_01_12a48.csv	Paymaster	1	67.6	0.171	19.6	0	1.207	0.024	0.237	1.212	0.580	4.86	<0.031	91.01	5.85	133	1397	214	6.28	0.81	3.04	9.15	93.5	5.12	27.6	51.2
2017_01_12a49.csv	Paymaster	1	69.4	0.085	19.6	0	0.586	<0.001	0.186	<0.100	0.749	4.93	<0.031	79.5	6.73	137	1114	170	4.26	0.451	2.157	6.75	83.7	3.38	25.3	41.7
2017_01_12a50.csv	Paymaster	1	68.7	0.077	19.6	0	0.368	0.002	0.088	0.59	2.41	3.72	<0.031	78.6	3.95	107	902	397	3.52	0.19	0.967	3.84	27.9	1.12	17.1	28.1
2017_01_12a51.csv	Paymaster	1	66.5	0.016	19.6	0	0.226	0.003	0.017	5.63	3.02	0.49	<0.031	415.07	0.908	7.46	184	845	0.019	0.007	<0.003	0.017	0.302	0.037	3.51	4.91
2017_01_12a57.csv	Paymaster	1	66.6	0.276	19.6	0	1.510	0.022	0.837	0.897	1.30	4.46	<0.031	167	24.3	140	7936	181	10.6	1.05	0.189	9.54	141	5.01	7.64	16.8
2017_01_12a60.csv	Paymaster	1	71.3	0.018	19.6	0	0.547	0.007	0.318	0.257	3.35	0.14	<0.031	59.4	7.27	4.05	145	349	0.17	<0.037	0.975	6.4	115	4.53	1.07	2.52
2017_01_12a63.csv	Paymaster	1	68.6	0.189	19.6	0	0.793	0.014	0.126	0.817	0.583	4.85	<0.031	71.07	6.71	146	1158	95.1	8.14	0.438	2.53	6.42	135	4.58	20.1	39.1
2017_01_12a64.csv	Paymaster	1	67.6	0.175	19.6	0	1.240	0.030	0.261	1.46	0.631	4.53	<0.031	456.7	5.86	118	938	204	7.08	0.6257	2.29	6.75	75.5	2.71	24.8	45.4
2017_01_13a05.csv	Crown	1	67.1	0.093	19.6	0	1.30	0.020	0.436	0.167	0.834	5.94	0.077	95.7	3.87	163	1335	281	7.38	0.687	2.79	9.11	68.1	3.75	44.1	86.3
2017_01_13a08.csv	Crown	1	68.3	0.104	19.6	0	0.812	0.007	0.233	0.205	0.564	5.69	0.020	56.8	5.56	145	1362	303	7.25	0.635	0.71	4.12	44.5	2.47	19.4	39.7
2017_01_13a10.csv	Crown	1	64.5	0.172	19.6	0	2.25	0.051	1.50	0.499	0.547	6.23	0.125	169.3	8.27	386	1640	143	10.2	1.15	4.57	9.45	131	6.29	61.7	136
2017_01_13a11.csv	Crown	2	67.6	0.098	19.6	0	0.791	0.009	0.280	0.026	0.385	6.74	<0.019	122.6	5.14	188	1216	99.1	7.51	0.486	2.07	1.51	9.69	0.48	5.88	14.8
2017_01_13a12.csv	Crown	2	68.2	0.099	19.6	0	0.826	0.011	0.203	0.111	0.627	5.86	<0.026	81.2	6.13	149	1136	214	6.92	0.69	3.7	1.36	94	3.72	9.19	22.4
2017_01_13a14.csv	Crown	2	68.2	0.105	19.6	0	0.926	0.015	0.218	0.242	0.797	5.33	0.043	60.5	4.93	137	1198	260	6.57	0.706	2.81	8.78	72.4	3.63	33.9	63.2
2017_01_13a16.csv	Crown	3	61.5	0.360	19.6	0	1.16	0.021	0.402	0.609	11.50	0.30	0.017	10.2	0.59	9.23	148	295	8.6	1.29	0.79	4.11	58.1	1.23	18.8	41.6
2017_01_13a18.csv	Crown	3	65.1	0.089	19.6	0	0.828	0.067	0.189	0.652	7.18	1.71	0.037	24.1	0.959	55.5	730	252	8.29	0.712	2.32	6.67	63.6	2.42	18.3	42.7
2017_01_13a21.csv	Crown	4	65.1	0.062	19.6	0	0.912	0.025	0.291	1.28	5.60	2.66	0.035	18.8	2.21	78.1	818	443	3.19	0.271	1.85	3.83	57.3	2.41	15.4	29.9
2017_01_13a24.csv	Crown	1	68.7	0.112	19.6	0	0.841	0.038	0.157	1.44	0.903	3.76	<0.026	47.01	3.43	124.7	1212	256	10.1	1.12	3.31	7.33	73.1	3.48	22.5	44.5
2017_01_13a25.csv	Crown	1	68.2	0.139	19.6	0	0.926	0.038	0.222	1.38	0.599	4.43	<0.028	41.1	3.35	113.9	989	299	7.55	0.812	1.99	5.72	67.9	2.61	27.04	50.5
2017_01_13a26.csv	Crown	1	66.0	0.075	19.6	0	0.818	0.013	0.206	0.28	5.38	3.18	<0.027	140	8.01	377	979	259	4.75	0.46	2.63	7.13	85.9	3.21	32.9	62.4
2017_01_13a41.csv	Krist	1	65.3	0.093	19.6	0	1.64	0.017	0.392	0.41	5.35	2.68	0.05	74.2	17.2	63.7	1714	576	4.11	0.202	2.86	7.77	98.6	3.64	28.5	53.05
2017_01_13a42.csv	Krist	1	66.0	0.149	19.6	0	1.49	0.029	0.381	1.01	2.20	4.68	0.03	21.4	3.98	102	1074	195	7.68	0.644	1.98	6.297	79.2	2.65	26.8	50.9
2017_01_13a43.csv	Krist	1	65.6	0.175	19.6	0	2.92	0.020	1.04	0.150	1.28	4.75	<0.059	87.1	9.86	73	166	202	5.82	0.73	0.66	9.67	47.1	1.29	5.0	9.31
2017_01_13a47.csv	Krist	1	65.5	0.058	19.6	0	2.97	0.023	1.03	0.283	0.63	5.42	<0.021	213	9.09	95	317	83	1.77	0.268	0.433	1.57	37.6	0.94	1.8	3.62
2017_01_13a48.csv	Krist	1	64.0	0.121	19.6	0	0.97	0.014	0.235	0.729	8.67	1.20	0.03	29.05	7.59	27	2479	381	6.15	0.532	2.664	8.26	91.6	3.61	26.4	48.1
2017_01_13a58.csv	Crown	1	68.1	0.123	19.6	0	1.24	0.009	0.279	<0.057	0.661	5.53	<0.077	97.1	4.81	144	1280	214	6.69	0.617	2.59	6.58	74.1	3.21	14.2	33.7
2017_01_13a64.csv	Crown	1	68.5	0.111	19.6	0	1.00	0.031	0.216	0.810	0.671	4.64	<0.016	38.6	3.68	122	999	267	7.78	0.666	2.052	6.59	47.3	1.94	30.8	57.7
2017_01_13a65.csv	Crown	1	68.2	0.144	19.6	0	1.23	0.023	0.235	0.348	0.669	5.09	<0.060	65.3	8.17	143	1064	184	11.1	0.729	2.53	8.04	25.2	1.06	33.8	65.09
2017_01_13a66.csv	Crown	1	68.6	0.117	19.6	0	1.01	0.025	0.235	0.289	0.591	5.04	0.03	43.7	6.1	150	1044	162	6.85	0.419	2.19	6.48	71.1	2.347	22.2	46.58
2017_01_13a67.csv	Crown	1	69.3	0.100	19.6	0	0.728	0.016	0.151	0.467	0.878	4.26	<0.019	248.1	4.63	134	1298	170	11.2	1.02	4.19	9.31	71.9	3.35	23.2	47.3
2017_01_13a71.csv	Crown	1	68.3	0.076	19.6	0	1.05	0.023	0.192	0.604	0.536	5.20	<0.031	47.2	3.22	105	933	296	5.87	0.38	3.16	2.3	1153	30.9	6.61	14.8
2017_01_13a72.csv	Crown	1	66.3	0.116	19.6	0	1.95	0.015	0.704	0.057	0.975	5.82	<0.018	163.8	8.48	145	1185	321	5.61	0.41	1.21	3	71	4.27	8.6	21.1

Table X - LA-ICPMS analyses of single melt inclusions in porphyry intrusions and porphyry fragments within volcanics (cont'd)

Ablation File	Host	Assemb.	Pr	Nd	Sm	Eu	Gd	Tb	Dy	Ho	Er	Tm	Yb	Lu	Y	Mo	W	Pb	Bi	Ag	Sn	Sb	Sc	V	Cr	Co	Ni
2017_01_12a08.csv	Paymaster	1	1.47	4.57	0.688	0.392	0.892	0.115	0.556	0.098	0.74	0.044	0.27	0.045	3.34	1.07	1.56	10.9	0.86	2.84	4.13	24.4	9.32	15.3	18.1	1.77	46.6
2017_01_12a09.csv	Paymaster	1	1.85	7.03	0.48	0.107	0.632	0.067	0.283	0.069	0.306	0.028	0.392	0.063	2.19	0.865	0.39	23.8	3.1	1.81	3.36	2.22	7.07	8.63	13.9	2.23	36.1
2017_01_12a10.csv	Paymaster	1	3.32	11.02	1.503	0.178	0.967	0.105	0.751	0.151	2.482	0.11	0.863	0.145	3.24	1.32	0.53	6.45	1.04	3.14	5.72	6.67	2.55	8.67	24.9	0.89	62.2
2017_01_12a11.csv	Paymaster	1	0.191	1.11	1.33	0.386	1.25	0.387	0.761	0.193	1.727	0.379	2.32	0.188	0.319	3.65	2.13	4.61	2.3	8.37	15.4	10.5	6.38	102	69.8	2.31	161.7
2017_01_12a13.csv	Paymaster	2	4.57	14.8	2.25	0.525	1.14	0.179	0.627	0.159	0.462	0.039	0.401	0.107	4.15	1.69	0.42	6.46	0.485	0.929	1.86	2.57	3.21	9.01	8.57	0.996	19.1
2017_01_12a14.csv	Paymaster	2	3.81	12.3	1.82	0.315	0.929	0.068	0.535	0.135	0.262	0.04	0.354	0.08	3.73	1.2	0.62	7.01	0.514	1.42	2.64	2.84	3.85	5.67	12.2	0.859	29.1
2017_01_12a15.csv	Paymaster	3	0.11	0.52	0.23	0.079	0.268	0.031	0.131	0.024	0.152	0.013	0.138	0.025	1.03	0.039	0.06	4.82	0.038	0.694	1.93	3.59	9.81	110	16.9	3.63	15.7
2017_01_12a16.csv	Paymaster	3	0.018	0.18	0.055	0.088	0.114	0.007	0.031	0.02	0.034	0.007	0.068	0.007	0.397	0.241	0.14	6.79	0.151	1.03	1.1	6.99	1.83	19.4	11.8	1.67	10.6
2017_01_12a19.csv	Paymaster	4	5.12	15.8	2.17	0.515	1.55	0.144	0.714	0.165	0.505	0.095	0.69	0.098	4.56	1.33	0.65	8.84	0.581	0.413	0.42	2.05	1.79	9.27	2	1.15	5.1
2017_01_12a18.csv	Paymaster	6	1.67	9.83	2.56	0.438	0.997	0.148	0.605	0.153	1.6	0.145	1.64	0.15	1.27	4.07	2.03	15.6	4.51	7.78	14.8	8.95	6.01	6.86	70.6	1.48	172
2017_01_12a23.csv	Paymaster	4	0.089	0.508	0.608	0.165	0.694	0.084	0.347	0.042	0.182	0.083	0.245	0.041	0.069	0.798	0.19	5.26	0.477	6.17	3.04	9.95	1.24	6.64	13.8	0.854	40.1
2017_01_12a23.csv	Paymaster	6	0.619	2.43	2.46	0.831	2.82	0.344	1.4	0.168	0.728	0.16	0.982	0.165	0.719	3.23	0.75	12	1.84	5.71	11.8	7.21	4.97	3.1	54.5	2.03	158
2017_01_12a29.csv	Paymaster	1	4.94	15.3	2.24	0.478	1.06	0.132	0.746	0.097	0.281	0.041	0.393	0.044	3.93	1.44	0.54	5.23	0.283	1.02	0.712	3.72	3.09	6.78	<1.23	1.23	<3.89
2017_01_12a30.csv	Paymaster	1	3.59	12.4	2.02	0.682	1.35	0.128	0.648	0.131	0.216	0.053	0.421	0.058	2.93	0.91	0.32	18.2	<0.084	3.45	<0.556	2.85	4.54	23.5	<2.69	0.987	<8.11
2017_01_12a31.csv	Paymaster	2	0.586	<1.83	<2.19	<0.259	<2.57	<0.307	<1.25	0.192	<1.716	<0.376	<0.758	<0.388	2.81	1.97	1.27	3.43	<1.92	<5.15	<10.8	<6.68	<5.93	7.51	<44.6	<1.77	<159
2017_01_12a32.csv	Paymaster	2	5.11	16.73	2.42	0.341	1.67	0.145	0.564	0.171	0.207	<0.100	0.348	<0.117	3.36	1.05	0.82	4.77	0.407	1.84	<2.45	4.62	5.4	6.22	<11.8	<0.569	<40
2017_01_12a33.csv	Paymaster	3	0.107	0.41	0.086	0.035	0.11	0.009	0.097	0.026	0.1	0.012	0.132	0.022	0.782	0.063	0.15	1.72	<0.014	0.206	1.96	0.7	9.58	114	12.2	2.26	10.4
2017_01_12a34.csv	Paymaster	3	3.9	12.8	1.72	0.367	1.01	0.123	0.601	0.111	0.338	0.049	0.362	0.061	3.71	1.47	0.43	7.25	0.278	0.708	0.48	1.73	2.79	13	0.51	1.28	1.31
2017_01_12a42.csv	Paymaster	x	3.44	10.6	1.71	0.248	0.931	0.13	0.533	0.101	0.3019	0.054	0.446	0.084	3.77	0.921	0.34	3.61	0.256	0.303	<0.638	1.3	4.3	27.4	5.74	6.95	22.9
2017_01_12a43.csv	Paymaster	x	1.5	3.62	0.76	0.189	<0.38	<0.069	<0.234	<0.029	0.276	<0.027	0.186	<0.028	0.627	0.312	<0.264	3.12	<0.364	<0.804	<1.69	<1.31	8.13	1.92	<8.31	0.73	<30.4
2017_01_12a44.csv	Paymaster	x	3.99	13.3	1.82	0.403	1.008	0.143	0.635	0.128	0.396	0.076	0.478	0.083	4.23	1.49	0.55	6.21	0.388	<0.706	<1.44	3.007	2.07	6.46	<6.33	0.75	<19.8
2017_01_12a43.csv	Paymaster	x2	4.53	15.4	2.36	0.402	1.252	0.169	1.19	0.266	1.1	0.172	1.33	0.331	8.26	1.25	0.53	8.46	0.305	0.463	<0.597	1.92	3.19	6.06	<2.91	0.89	<10.5
2017_01_12a47.csv	Paymaster	1	8.51	26.1	3.34	0.79	2.06	0.249	0.82	0.154	0.455	0.035	<0.166	0.041	3.2	1.54	1	9.11	1.06	1.75	<2.27	7.69	7.68	8.95	11.2	0.57	<27.9
2017_01_12a48.csv	Paymaster	1	5.39	17.1	2.02	0.506	1.48	0.205	1.07	0.12	0.812	0.113	0.336	0.081	4.39	1.51	0.57	8.41	<0.4039	<1.04	<2.08	2.35	4.16	8.11	<10.02	1.03	<22.2
2017_01_12a49.csv	Paymaster	1	4.26	15.6	5.46	1.35	2.78	0.193	1.58	0.319	<0.994	0.11	0.936	0.157	5.66	<0.766	0.84	7.47	<1.27	3.7	<7.39	<4.47	2.7	2.92	<35.4	<1.30	<91.1
2017_01_12a50.csv	Paymaster	1	2.94	9.59	1.83	0.861	1.32	0.209	0.611	<0.084	0.403	0.113	3.08	<0.082	2.5	<0.520	<0.372	8.01	<0.808	<2.2	<4.23	3.11	4.35	2.69	<21.4	<0.671	<61.6
2017_01_12a51.csv	Paymaster	1	0.4	1.21	0.162	0.666	0.055	0.0102	0.037	0.004	<0.036	<0.003	0.021	<0.008	0.116	<0.056	<0.0142	7.51	<0.101	0.141	<0.29	1.27	1.6	<0.07	<1.57	0.044	<3.69
2017_01_12a57.csv	Paymaster	1	1.92	7.67	1.1	0.145	0.807	0.116	0.731	0.117	0.647	0.0571	0.542	0.114	3.89	0.176	<0.048	9.19	<0.157	11.1	<0.94	2.42	3.3	48.5	<4.15	2.15	<14.1
2017_01_12a60.csv	Paymaster	1	0.229	0.972	0.328	0.032	<0.237	<0.043	<0.144	0.02	<0.158	<0.014	<0.265	<0.014	0.461	<0.194	<0.201	4.23	<0.154	<0.483	<1.05	12.5	1.4	10.2	<5.35	1.18	<18.9
2017_01_12a63.csv	Paymaster	1	3.84	15.22	2.03	<0.303	<1.23	0.207	0.88	0.229	1.097	<0.144	1.21	<0.149	7	1.61	1.07	5.64	<0.630	<1.92	<4.38	5.81	<2.45	6.32	<21.7	1.1	<73.4
2017_01_12a64.csv	Paymaster	1	4.71	14.03	1.71	0.4	1.23	0.124	0.906	0.142	0.312	0.065	0.298	0.037	4.18	1.13	0.37	5.34	0.191	0.59	<0.501	2.21	1.47	7.68	<2.56	1.25	<8.55
2017_01_13a05.csv	Crown	1	9.24	28.1	2.57	0.62	1.79	0.147	0.832	0.177	0.497	0.038	0.728	0.112	4.03	0.119	0.45	15.1	<0.161	<0.282	<0.707	<0.532	4.32	8.56	<3.27	2.27	<9.10
2017_01_13a08.csv	Crown	1	4.31	15.8	1.24	0.46	1.11	0.046	0.49	0.075	0.327	0.031	<0.236	0.026	2.1	0.211	0.32	12.1	0.255	<0.560	<1.15	<0.766	2.38	4.63	<5.72	15.8	<12.9
2017_01_13a10.csv	Crown	1	16.2	53.4	6.17	0.78	3.17	0.385	1.42	0.235	0.864	0.08	0.556	0.132	6.37	0.265	0.5	16.5	0.193	<0.387	1.45	0.8	4.16	50.6	<3.93	4.51	<10.1
2017_01_13a11.csv	Crown	2	1.96	7.49	1.86	0.544	1.04	0.068	0.16	<0.048	<0.247	<0.045	<0.161	<0.047	0.58	<0.183	<0.219	2.64	<0.296	<0.583	<1.25	<0.816	4.66	10.8	<5.37	0.721	<18.2
2017_01_13a12.csv	Crown	2	1.87	5.94	0.86	0.558	0.645	0.167	0.845	0.217	0.846	0.0795	0.445	0.138	5.38	0.495	0.33	7.76	<0.345	<0.839	<1.57	<1.02	1.44	4.13	<7.54	0.983	<27.5
2017_01_13a14.csv	Crown	2	6.78	20.6	2.87	0.727	1.48	0.208	1.13	0.111	0.568	0.096	0.798	0.162	5.86	0.442	0.32	10.1	0.252	<0.374	<0.831	<0.621	<0.320	4.37	<4.03	1.01	<12.1
2017_01_13a16.csv	Crown	3	4.75	17.2	2.69	0.543	1.37	0.136	0.506	0.077	0.169	0.026	0.195	0.036	1.86	0.453	0.94	14.6	<0.011	4.6	0.137	1.01	0.447	22.8	2.44	1.23	1.3
2017_01_13a18.csv	Crown	3	4.15	14.4	2.41	0.642	1.76	0.257	1.26	0.268	0.796	0.133	0.928	0.132	8.27	0.271	0.22	16.7	0.126	<0.071	0.383	0.156	0.936	3.48	<0.724	14.4	<3.08
2017_01_13a21.csv	Crown	4	3.27	10.3	1.59	0.371	1.13	0.102	0.566	0.146	0.362	0.057	0.447	0.082	4.01	0.619	0.64	5.1	0.104	<0.137	<0.348	<0.226	<0.178	4.35	<1.37	0.95	<6.07
2017_01_13a24.csv	Crown	1	4.89	17.4	2.6	0.7	2.46	0.288	1.737	0.333	1.14	0.177	1.41	0.202	10.7	0.71	0.32	7.15	0.324	0.869	1.34	1.03	1.564	3.98	4.98	0.55	26.9
2017_01_13a25.csv	Crown	1	5.16	15.6	2.28	0.514	1.1	0.145	0.748	0.103	0.257	0.054	0.892	0.089	4.89	0.484	0.15	3.96	0.281	0.628	1.49	1.07	0.797	3.84	7.09	1.12	27.4
2017_01_13a26.csv	Crown	1	6.35	20.9	2.56	0.502	1.37	0.186	1.056	0.141	0.446	0.0601	0.449	0.088	5.71	0.76	0.19	2.28	0.387	0.591	1.43	1.03	1.4	4.47	6.33	0.68	26.7
2017_01_13a41.csv	Krist	1	5.44	16.8	2.34	0.415	1.45	0.227	0.905	0.182	0.646	0.072	0.528	0.133	4.69	1.41	0.22	4.13	0.46	0.92	2.15	1.45	2.52	8.13	8.73	1.25	35.3
2017_01_13a42.csv	Krist	1	4.74	14.7	1.81	0.426	0.956	0.1017	0.574	0.102	0.359	0.049	0.465	0.045	3.46	0.605	0.33	4.25	0.224	0.476	0.422	0.302	2.58	8.3	1.31	2.92	4.7
2017_01_13a43.csv	Krist	1	0.786	2.06	0.631	0.182	0.594	0.088	0.143	0.036	0.5	0.0343	0.213	0.089	0.143	0.3	0.42	3.77	0.474	0.974	2.72	2	1.98	16.5	12.7	6.778	54.1
2017_01_13a47.csv	Krist	1	0.334	0.92	0.163	0.137	0.431	0.033	0.094	0.024	0.196	0.057	0.266	0.059	0.287	0.2	0.11	2.52	0.205	0.511	1.09	0.726	3.85	6.28	5.69	5.78	21.3
2017_01_13a48.csv	Krist	1	5.3	15.08	2.06	0.477	1.189	0.143	0.783	0.155	0.302	0.08	0.681	0.042	3.949	1.01	0.42	4.09	0.357	0.42	0.82	0.478	1.99	6.02	3.99	1.1	13.9
2017_01_13a58.csv	Crown	1	3.3	12.1	1.31	0.508	1.05	0.126	0.956	0.065	0.64	0.061	<0.835	0.141	2.23	0.635	0.78	6.45	<1.03	<2.36	<4.64	<3.05	3.25	4.23	<26.9	0.831	<65.6
2017_01_13a64.csv	Crown	1	6.03	18.6	2.38	0.547	1.8	0.211	0.729	0.155	0.429	0.053	0.427	0.063	5.51	0.581	0.25	4.63	0.293	<0.367	<0.862	<0.46	1.9	4.27	<4.20	1.229	<17.5
2017_01_13a65.csv	Crown	1	6.66	19.8	2.35	0.491	1.6	0.106	0.733	0.158	0.657	0.035	<1.02	0.096	4.39	0.553	0.56	3.9	<0.557	<1.59	<2.90	<1.90	1.59	4.78	<14.4	1.129	<54.3
2017_01_13a66.csv	Crown	1	5.23	15.9	2.19	0.547	1.33	0.1287	0.796	0.142	0.496	0.055	0.577	0.062	5.004	0.682	0.22	2.56	<0.269	<0.590	<1.39	<0.83	1.78	4.71	<6.58	1.07	<26.7
2017_01_13a67.csv	Crown	1	5.42	18.9	3.88	0.524	2.3	0.317	1.79	0.275	0.961	0.14	1.23	0.226	11.2	0.437	0.07	3.73	0.259	<0.2836	<0.991	<0.524	3.22	3.3	<4.36	0.586	<18.3
2017_01_13a71.csv	Crown	1	1.65	6.48	1.65	0.41	1.57	0.319	2.26	0.571	1.88	0.427	3.98	0.69	14.9	0.261	0.17	3.94	0.696	<0.736	<1.91	<1.11	2.15	2.35	<9.24	1.31	<31.3
2017_01_13a72.csv	Crown	1	2.71	10	1.65	0.495	0.806	0.098	0.783	0.183	0.485	0.078	0.473	0.089	4.3	0.29	0.17	12.5	0.259	<0.447	1.29	0.889	2.07	44.1	5.36	3.17	<17.7

6.0 Acknowledgements

I would Like to thank Dr. Jacob Hanley for his continuous mentorship throughout my undergraduate degree and for his support and patience. I would also like to thank all my friends at the Saint Mary's University Geology Dept. for their support and making my time at Saint Mary's University a memorable one, especially Mehran, Alexis, Amara, Zach, Andras, Anthony, Glen, Jordan, Gaggan, Raj, Travis, Mahoney, Dan, Devan, Wilson, Olga, Cathy and Corwin. I would also like to thank Dr. Zoltan Zajacz and his wife Sasha for their assistance in acquiring melt inclusion data that has been fundamental for this study. I would also like to thank Xiang Yang for his assistance in operation of the BSE-SEM at Saint Mary's University. My sincerest thanks to Pierre Bousquet for enabling me to collect samples for BSE-SEM analysis. Finally, I would like to thank my parents for being the best parents that they could ever be and my sister for not only being an amazing sibling but also a great friend.

7.0 References

Audétat, A., Pettke, T., Heinrich, C.A., and Bodnar, R.J. 2008. Special paper: the composition of magmatic-hydrothermal fluids in barren and mineralized intrusions. Economic Geology, **103**: 877-908.

Audetat, A., Gunther, D., and Heinrich, C.A. 1998. Formation of a magmatic-hydrothermal ore deposit: insights with LA-ICP-MS analysis of fluid inclusions. Science (New York, N.Y.), **279**: 2091-2094.

Davies, J.F., 1977, Structural reinterpretation of the Timmins Mining area, Ontario: Canadian Journal of Earth Science. v. 14. pp. 1046-1053.

Davies, J.F., and Luhta, L.E., 1978, An Archean "porphyry-type" disseminated copper deposit, Timmins, Ontario: Econ. Geol., v. 73, p. 383-396.

Dinel, E., Fowler, A.D., Ayer, J., Still, A., Tylee, K., and Barr, E. 2008. Lithogeochemical and stratigraphic controls on gold mineralization within the metavolcanic rocks of the Hoyle Pond Mine, Timmins, Ontario. Economic Geology, **103**: 1341-1363.

Dubé, B., and Gosselin, P., 2007, Greenstone-hosted quartz-carbonate vein deposits, *in* Goodfellow, W.D., ed., Mineral Deposits of Canada: A Synthesis of Major Deposit-Types, District Metallogeny, the Evolution of Geological Provinces, and Exploration Methods: Geological Association of Canada, Mineral Deposits Division, Special Publication no. 5. pp. 49-73.

Ferguson, S., Buffam, B., Carter, O., Griffis, A., Holmes, T., Hurst, M., Jones, W., Lane, H., and Longley, C. 1968. Geology and ore deposits of Tisdale Township, District of Cochrane. Ontario Department of Mines Geological Report 58. .

Ferguson, S.A., 1968, Geology and ore deposits of Tisdale Township: Ontario Department of Mines Geological Report 58. pp. 177.

Gray, M.D., and Hutchinson, R.W. 2001. New evidence for multiple periods of gold emplacement in the Porcupine mining district, Timmins area, Ontario, Canada. Economic Geology, **96**: 453-475.

Groves, D.I., Goldfarb, R.J., Hart, C.J.R., and Robert, F., 2003, Gold deposits in metamorphic belts: Overview of current understanding, outstanding problems, future research, and exploration significance: Economic Geology. v. 98. pp. 1-29.

Groves, D.I., Goldfarb, R.J., Gebre-Mariam, M., Hagemann, S.G., and Robert, F., 1998, Orogenic gold deposits: A proposed classification in the context of their crustal distribution and relationship to other gold deposit types: Ore Geology Reviews. v. 13. pp. 7–27.

Goldfarb, R.J., Baker, T., Dube, B., Groves, D.I., Hart, C.J., and Gosselin, P. 2005. Distribution, character, and genesis of gold deposits in metamorphic terranes. Economic Geology 100th anniversary volume, 40.

Klemm, L.M., Pettke, T., and Heinrich, C.A. 2008. Fluid and source magma evolution of the Questa porphyry Mo deposit, New Mexico, USA. Mineralium Deposita, **43**: 533-552.

MacDonald, P.J. 2010. The geology, lithogeochemistry and petrogenesis of intrusions associated with gold mineralization in the Porcupine Gold Camp, Timmins, Canada. *In* Masters Abstracts International, Vol. 48.

Pyke, D. 1982. Geology of the Timmins area, District of Cochrane. Ontario Ministry of Natural Resources.

Spooner, E.T.C., 1991. The magmatic model for the origin of Archean Au-quartz vein ore systems: An assessment of the evidence, Brazil Gold '9, E.A Ladeira (ed). pp. 313-318.

Spooner, E.T.C., 1992. Magmatic Sulphide/Volatile interation as a mechanism for producing chalcophile element enriched, Archean Au-quartz, epithermal Au-Ag and Au skarn hydrothermal ore fluids, Ore Geology Reviews. v.7. pp. 359-379

Tomlinson, K.Y., 2004. A Review of Greenstone Belts in the Superior Province and the Evolution of Archean Tectonic Process, http://www.lithoprobe.ca/Contributed%20Abstracts/Poster%20Presentation/Tomlinson%20Lith2004.pdf. Web. February 9, 2010.

Winter, J.D., 2001. An Introduction to Igneous and Metamorphic Petrology, Ch. 18. Pretence-Hall Inc., N.J. pp. 343-361.

Zajacz, Z.., Halter, W.E., Pettke, T., Guillong, M., 2008. Determination of fluid/melt partition coefficients by LA-ICPMS analysis of co-existing fluid and silicate melt inclusions: Controls on element partitioning. Science Direct. v. 72. pp. 2169-2197